ErbB2/HER2 governs CDK4 inhibitor sensitivity and timing and irreversibility of G1/S transition by altering c-Myc and cyclin D function

Ayaka Nagasato-Ichikawa[1], Ken Murakami[1], Kazuhiro Aoki[2,3], and Mariko Okada[1]*

[1]Laboratory for Cell Systems, Institute for Protein Research, Osaka University, Suita, Osaka 565-0871, Japan

[2]Exploratory Research Center on Life and Living Systems (ExCELLS), National Institutes of Natural Sciences, Okazaki, Japan; National Institute for Basic Biology, National Institutes of Natural Sciences, Okazaki, Japan; Department of Basic Biology, School of Life Science, SOKENDAI (The Graduate University for Advanced Studies), Okazaki 444-8787, Japan

[3]Graduate School of Biostudies, Kyoto University, Kyoto 606-8501, Japan

*Corresponding author: mokada@protein.osaka-u.ac.jp

Competing interests: The authors declare that they have no competing interests.

Abstract

Cell cycle entry and the irreversible transition from the G1 to S phase are crucial for mammalian cell proliferation. Among the ErbB family, the ErbB2/HER2 receptor is a key driver of cancer growth. However, the quantitative mechanisms underlying the ErbB2-mediated G1/S transition remain unclarified. Here, we performed an extensive time-course analysis of high and low ErbB2-expressing breast cancer cells to describe the regulatory mechanisms of the ErbB2-mediated G1/S transition. Live-cell imaging using cell cycle reporters revealed that the G1/S transition occurs 20 h after ErbB2 activation, driven primarily by the cyclin D1/CDK4–RB axis. Hsp90 is regulated by CDK4 activity and controls the stability of ErbB2 protein in a time-dependent manner. CDK4 inhibitor treatment arrested the cell cycle in most cells; a subpopulation showed a 25-h delay in G1/S entry associated with enhanced c-Myc activation. In high ErbB2-expressing cells, CDK4 inhibition led to c-Myc overactivation, a rapid decrease in cyclin D1 expression, and cell cycle arrest. Overall, we demonstrate how ErbB2 receptor levels modulate the roles of cyclin D1 and c-Myc in the G1/S transition and suggest that variations in ErbB2 levels within breast cancer tissues confer heterogeneous sensitivity to CDK4 inhibitors, potentially complicating treatment.

Main text:

Introduction

The initiation of the cell cycle and subsequent transition from the G1 to S phase are regulated by a complex molecular network involving the formation of a cyclin D1/CDK4 protein complex (*1–3*). Understanding the regulation of the G1/S transition by mitogenic signals is fundamental for comprehending cell biology and developing cancer treatments that overcome drug resistance. For example, based on the important role of cyclin D1 overexpression for

enhancing breast cancer cell proliferation (*4*), various cell cycle inhibitors targeting CDK4 have been developed to treat breast cancer (*5*, *6*).

Breast cancer can be classified into four subtypes based on the expression of estrogen receptors (ERs), progesterone receptors, and ErbB2 (HER2) receptors: luminal A (ER^+ and $HER2^-$), luminal B (ER^+ and $HER2^+$), ErbB2/HER2-positive (ER^- and $HER2^+$), and triple-negative (ER^- and $HER2^-$) (*7–9*). CDK4 inhibitors (CDK4is) have been used to treat the luminal A subtype (*5*, *10*), but long-term administration has led to drug resistance (*11–17*). ErbB2 tyrosine kinase activity, commonly elevated in malignant breast cancer, increases cyclin D1 levels (*18*, *19*). Stimulation of ErbB2 receptors activates the MAPK/ERK and PI3K/AKT signaling pathways, leading to the rapid induction of early-response genes such as *c-fos* and *c-myc* (*20–22*)—key regulators of cyclin D1 and CDK4 expression (*22–24*). Both c-Myc and cyclin D1 are involved in the G1/S transition, though they appear to have distinct roles (*25*). Therefore, we speculated that the small population of high ErbB2-expressing cells in the luminal A subtype may contribute to CDK4i resistance by rewiring the G1/S network during the early stages of drug treatment. However, the molecular mechanisms by which ErbB2 affects the G1/S transition following CDK4i treatment remain unclear.

The G1/S transition typically involves signal-dependent and -independent processes, which are distinguished by the restriction (R) point (*2*, *26*). The mitogenic signal primarily regulates the expression and activation of cyclin D1/CDK4, which phosphorylates retinoblastoma protein (RB) prior to the R point. Thus, this signal-dependent process is primarily driven by the cyclin D1/CDK4-RB axis (*2*). The phosphorylation of RB (p-RB) activates E2F1, promoting the expression of its target genes, including cyclin E. Cyclin E then forms a complex with CDK2, which further phosphorylates p-RB, resulting in a fully phosphorylated state (pp-RB). Fully activated pp-RB enhances E2F1 activity, creating a mitogen-independent cyclin E/CDK2–RB–E2F1 positive feedback loop (*27*, *28*). However, the expression and

68 stability of c-Myc are modulated by external signals (*29*), and c-Myc directly influences
69 E2F1 promoter activity (*30*). Consequently, the core machinery of cyclin E/CDK2–RB–E2F1
70 is considered to be indirectly regulated by mitogenic signals.
71 ERK controls the expression of c-Myc and cyclin D1 (*31*, *32*), and AKT regulates their
72 protein stability (*31*, *33*). However, p27 expression, which plays a crucial role in the
73 accumulation of cyclin D1 and CDK4 during the G1 phase (*34*), is repressed by c-Myc (*35*).
74 Since the ErbB2 receptor activates the ERK and AKT pathways at different magnitudes (*36*),
75 different levels of ErbB2 may modulate the core machinery of the G1/S network and,
76 consequently, the timing of cell cycle entry through modulation of cyclin D1 and c-Myc.
77 Therefore, investigating the ratio of c-Myc to cyclin D1 at the single-cell level may elucidate
78 their specific functions in the G1/S transition and the regulatory role of the ErbB2 receptor.
79 In the present study, we used representative luminal A subtype cell lines (MCF-7 and T47D),
80 which express low levels of the ErbB1 receptor (EGFR) and high levels of the ErbB3
81 receptor (*22*, *36*, *37*). ErbB2 is an orphan receptor that is activated by heterodimerization with
82 ErbB3, ErbB4, or EGFR (*21*). Stimulation with the ErbB3 ligand, heregulin (HRG), triggers
83 the heterodimerization of ErbB2 and ErbB3, thereby activating the ERK and AKT pathways
84 (*36*). We conducted time-course protein phosphorylation profiling after HRG stimulation,
85 fluorescent ubiquitination-based cell cycle indicator (FUCCI) live-cell imaging for cell cycle
86 dynamics, and transcriptomic/epigenetic studies to identify key transcription factors during
87 CDK4 inhibition. We evaluated the role of ErbB2 in regulating the timing and irreversibility
88 of the G1/S transition, revealing the molecular mechanism underlying heterogeneous CDK4
89 inhibitor sensitivity.
90

91 **Results**

92 **G1/S transition occurs approximately 20 h after HRG stimulation**

93 First, we used FUCCI (*38*) live-cell imaging to analyze the cell cycle dynamics in MCF-7 or
94 T47D cells after HRG stimulation (Fig. 1A) and analyzed the distribution of each cell cycle
95 phase in the presence or absence of HRG for up to 72 h in MCF-7 cells (Fig. 1B–D). HRG
96 stimulation began to significantly increase the proportion of S/G2/M-phase cells after 24 h
97 compared to the control. The number of nuclei, serving as a proxy of cell number, increased
98 1.4-fold after 48 h, suggesting that HRG stimulation enhances cell proliferation. Conversely,
99 control cells showed a gradual increase in the proportion of S/G2/M cells, but there was no
100 increase in the number of nuclei, suggesting cell cycle arrest during the S/G2/M phase. To
101 further examine the times of transition for each cell cycle phase, we performed single-cell
102 tracking and quantified the distribution of the cell cycle phases (Fig. 1E; Fig. S1A, B). The
103 G1/S transition occurred at 19.0 ± 7.2 h after HRG stimulation. In comparison, the S/G2 and
104 M/G1 transitions occurred at 32.5 ± 9.3 h and 39.4 ± 8.7 h, respectively (Fig. 1F). These
105 findings suggested that most cells entered the S phase approximately 20 h after HRG
106 stimulation, with some intercellular variability.

107 **CDK4 and cyclin D1 proteins are expressed in a time-dependent manner at the G1/S**
108 **transition**

109 We further examined the signaling dynamics of the ErbB2, AKT, and ERK pathways (*21*, *39*)
110 following HRG stimulation (Fig. 2A, B). p-ErbB2, p-AKT, and p-ERK levels decreased after
111 peaking within 30 min, and remained present until the S/G2 transition point (32.5 ± 9.3 h).
112 Although c-Fos protein levels peaked within 2 h and quickly reduced to basal levels, p-c-Fos
113 showed similar dynamics to those of p-ERK, a critical regulator of p-c-Fos (*22*). Following
114 ErbB2 activation, p-AKT, p-ERK, and p-c-Fos levels remained consistent whereas c-Myc and
115 p-c-Myc (Ser^{62}) levels decreased around the time of the G1/S transition (19.0 ± 7.2 h).
116 We estimated the timing of the R point based on the dynamics of cell cycle regulatory
117 proteins (Fig. 2C, D; Fig. S2A, B). The protein levels of cyclin D1 and CDK4 started to

118 increase shortly after HRG stimulation, peaked at approximately 20 h (G1/S transition point),
119 and then remained consistent until the S/G2 transition (Fig. 2D), consistent with the trend in
120 p-RB (Thr^{373}) expression (*40*). p-RB (Ser$^{807/811}$) showed a monotonic increase similar to
121 cyclin E (Fig. S2A, B), suggesting the involvement of CDK2-mediated S phase progression
122 (Fig. S2A, B). Since the R point is found just before the G1/S transition, we estimated that it
123 occurs at 12–16 h, when the E2F1 protein level is highly elevated. Thus, our results
124 substantiate that cyclin D1/CDK4 maintains RB phosphorylation near the R point, which is a
125 critical initial step toward the G1/S transition associated with HRG-induced ErbB2
126 activation.

127 **A population subset enters the cell cycle even after CDK4 inhibition**

128 We confirmed the involvement of cyclin D1/CDK4 in the HRG-stimulated G1/S transition.
129 Cells were treated with CDK4i at 12 h after HRG stimulation (before the R point; Fig. S3A,
130 B). As ERK activates cyclin D1 expression and AKT inhibits its degradation (*41*), we used
131 AKT inhibitor (AKTi) and MEK inhibitor (MEKi), which have comparable inhibitory effects
132 on cyclin D1 expression (Fig. S3A, B), as CDK4is. We examined the proportions of cells in
133 each cell cycle phase at 32 h and 72 h after HRG stimulation (Fig. 3A, B). At 32 h, fewer
134 cells treated with CDK4i (13.8%), AKTi (7.05%), or MEKi (13.8%) were in the S/G2/M
135 phase compared to non-treated cells (29.2%). At 72 h, AKTi (9.85%) and MEKi (5.50%)
136 reduced the proportion of cells in the S/G2/M phase, but CDK4i (17.7%) did not. At this time
137 point, the number of nuclei was significantly reduced by AKTi and MEKi but not CDK4i
138 (Fig. 3C). This finding indicated that AKTi and MEKi induced the growth of most cells,
139 whereas a significant subpopulation of cells were not affected by CDK4i, suggesting that
140 additional mechanisms maintain cell cycle functionality in the absence of CDK4.
141 To investigate the distinct mechanisms associated with CDK4i, we analyzed the correlations
142 between the times to the G1/S and M/G1 transitions up to 72 h for the different treatments

143 (Fig. 3D). Cells non-responsive to CDK4i showed significantly delayed G1/S transition times
144 (49.5 ± 13.2) of ~25 h compared to the control (24.7 ± 5.7), which tended to be longer than
145 under AKTi (39.6 ± 14.8) and MEKi (26.6 ± 11.5; Fig. 3D). We analyzed the slope (s),
146 representing the effect on the subsequent cell cycle duration after G1/S transition, and
147 intercept (i), representing the time to the M/G1 transition, and observed a lower slope (s =
148 0.56) and higher intercept (i = 37) under CDK4i than under AKTi (s = 1.0, i = 19), MEKi (s =
149 0.95, i = 17), and control conditions (s = 1.0, i = 17). Thus, Pearson's correlation coefficients
150 (R) were significantly lower for CDK4i (0.76) than for AKTi (0.91), MEKi (0.95), and
151 control conditions (0.84). This observation implied that the duration of the G1/S to G2/M
152 phase might not be uniformly controlled only by CDK4i and phase-specific regulation might
153 occur.
154 The CDK4i condition showed a clear negative correlation between the time to G1/S transition
155 and duration of the S/G2/M phase (Fig. 3E). We divided the cell population into the early and
156 late groups based on the median time of each G1/S transition (CDK4i, 49.5 ± 13.2; AKTi,
157 39.6 ± 14.8; MEKi, 26.6 ± 11.5; Control, 24.7 ± 5.7) and compared the duration of each S,
158 G2, and M phase (Fig. S3C). The mean duration of S/G2/M differed significantly between
159 the early (22.3 ± 7.2) and late (15.8 ± 2.4) groups, with a 6-h difference observed in the
160 CDK4i groups. Thus, in this CDK4i-specific response, the majority of CDK4i non-
161 responsive cells showed a long G1/S and short S/G2/M phase (Fig. 4A). We observed that
162 CDK4i non-responsive T47D cells (another luminal A cell line), which normally express
163 ErbB2 at a level three times higher than MCF-7 cells (Fig. S3D, E), also required a long time
164 (32.6 ± 12.2 h) to reach the G1/S transition compared to the control (21.62 ± 6.2 h; Fig. S3F).
165 **CDK4i enhances c-Myc transcriptional activity via H3K27Ac modification**
166 Given the distinct cell cycle kinetics observed under CDK4 inhibition (Fig. 4A), we
167 performed transcriptome and epigenetic analyses to investigate the molecular mechanisms

168 responsible for cell cycle regulation post CDK4 inhibition. To elucidate the changes in gene
169 expression patterns, we added CDK4i 12 h after HRG stimulation and performed a time-
170 course analysis of mRNA expression [0 (control), 2, 4, 8, 12, 16, 20, 24, and 28 h after HRG]
171 as well as H3K27Ac and H3K4me1 modification [12 (control), 16, 20, 24, and 28 h after
172 HRG]. First, active transcription factors were predicted at each time point with DoRothEA
173 using RNA-seq data (*42*) (Fig. S4A). mRNAs corresponding to key transcription factors,
174 such as *Myc*, AP-1 family (*Jun* and *Fos*), *EGR1*, *NFKB1*, and *STAT3*, which are known to
175 promote cell cycle progression (*21*, *23*, *25*, *43*, *44*), were highly upregulated 16 h after HRG
176 stimulation.
177 Motif-enrichment analysis was performed to confirm the binding of these transcription
178 factors to the promoter regions. Here, we defined the regions without overlap between the
179 H3K27Ac and H3K4me1 peak signals as the active promoter regions (*45*, *46*). E-box
180 sequences (CANNTG) (*47*) were enriched in the promoter regions at all time points
181 following CDK4i treatment (Fig. 4B; Fig. S4B, C). Given that c-Myc binds with E-box
182 sequences (*48*), we focused on its role in G1/S transition. Control cells showed lower c-Myc
183 protein and p-c-Myc (Ser^{62}) levels near the R point (12–16 h after HRG) than during the early
184 time point (0–2 h after HRG; Fig. 2A, B). Additionally, gene set enrichment analysis (GSEA)
185 using normalized enrichment scores (*49*) did not show any significant enrichment of c-Myc-
186 target genes during 12–16 h (Fig. 4C). However, CDK4i induced a significant enrichment of
187 c-Myc-target genes at 16 h after HRG stimulation, followed by a downregulation at 24–28 h
188 compared to that in the control (Fig. 4D). We analyzed the temporal expression of cell cycle-
189 related c-Myc-target genes.
190 Focusing on genes exhibiting a higher abundance of H3K27Ac modifications in their
191 promoter than their enhancer region (Fig. S4D). *CCNE1* expression was significantly
192 enhanced 16 h after HRG stimulation and CDK4i treatment, whereas the expression of

193 *CCND1*, *CDK1*, *CDC25A*, *E2F2*, *E2F3*, and *CDKN1B* showed delayed upregulation during
194 20–28 h. These findings suggested that CDK4 inhibition alters the H3K27Ac levels in the
195 promoter regions of c-Myc-target genes near the R point, promoting the expression of cell
196 cycle-related genes. Therefore, when the G1/S transition, originally regulated by the cyclin
197 D1 and CDK4 complex, is inhibited by CDK4i, it is maintained by an alternative pathway
198 facilitated by c-Myc activity.
199 We confirmed whether the delayed G1/S entry following CDK4i treatment was due to c-Myc
200 activation by testing the effects of an inhibitor of c-Myc transcriptional activity (EN4). In
201 both MCF-7 and T47D cells after 30 h, the combination of CDK4i and EN4 increased the
202 proportion of G1-phase cells and decreased the number of S/G2/M-phase cells in a dose-
203 dependent manner (Fig. 4E–H), while no change was observed with EN4 alone (Fig. S4E–H).
204 These results suggested that the transcriptional activity of c-Myc promotes the delayed G1/S
205 entry and escape from cell cycle arrest in response to CDK4 inhibition.
206 To further validate these findings using clinical data, we retrospectively analyzed the
207 microarray data from patients with luminal A subtype breast cancer who received long-term
208 (16 weeks, $n = 23$) or short-term (4 weeks, $n = 26$) CDK4/6i therapy (*50*). *PCNA*, a target
209 gene for both c-Myc and E2F involved in DNA replication during G1/S transition, showed a
210 0.5 $\log_2$ fold change (FC) between the long-term and short-term treatment groups (Fig. 4I).
211 *PCNA* mRNA expression increased after CDK4i treatment from 4 to 12 h (16–24 h after
212 HRG) relative to the control (Fig. 4J). Collectively, these findings suggested that CDK4
213 inhibition-induced epigenetic modifications activated c-Myc-target genes, ultimately
214 promoting cell cycle maintenance in cancer cells (Fig. 4K).
215 **CDK4i induces ErbB2 degradation and delays G1/S transition**
216 c-Myc is known to promote G1/S transition and cell proliferation (*25*, *35*). Therefore, if the
217 transcriptional activity of c-Myc is enhanced by CDK4i at 16 h, the time to G1/S transition is

218 unlikely to be extended; however, the G1/S transition was prolonged in our study (Fig. 3D, E;
219 Fig. 4A). We found that the levels of phosphorylated ErbB2, ERK, and AKT, which induce *c-*
220 *Myc* mRNA expression and stabilize the c-Myc protein, decreased after CDK4 inhibition,
221 leading to a slight reduction in c-Myc protein level (Fig. 5A, B). Although the expression of
222 ErbB2 was lower in MCF-7 and T47D cells than in HER2-positive cells, growth in these cell
223 lines is mainly dependent on ErbB2-ErbB3 heterodimer activation after HRG stimulation
224 given their low expression of EGFR and ErbB4 (*37*). This finding suggested that the CDK4i-
225 induced downregulation of the ErbB2 pathway may prolong the G1/S transition in MCF-7
226 and T47D cells (Fig. 3D; Fig. S3F). To investigate this mechanism, we focused on the
227 Hsp90-chaperone system, particularly with respect to the stability and maturation of nascent
228 ErbB2. As WT MCF-7 cells naturally express low levels of ErbB2, we constructed MCF-7
229 cells with moderate overexpression of ErbB2 (Fig. S5A, B). After confirming the unaltered
230 protein expression of ErbB2, PY100 (pan-tyrosine phosphorylation for estimating p-ErbB2
231 level), and Hsp90 under CDK4i (Fig. S5C–G), we examined the co-localization patterns
232 using Mander's and Pearson's coefficients. Compared to control conditions, CDK4i reduced
233 the co-localization of Hsp90 with ErbB2 or PY100 (Fig. 5C–F). No significant difference
234 was observed in the total number of nuclei (Fig. S5H, I). These results suggested that CDK4i
235 inhibits the interaction between Hsp90 and ErbB2, leading to ErbB2 misfolding. In addition,
236 ErbB2 protein expression was reduced 20 h after HRG stimulation (Fig. 5G, H; Fig. S5J);
237 however, *ErbB2* mRNA levels did not change regardless of CDK4i treatment (Fig. S5K).
238 Therefore, we investigated whether the downregulation of ErbB2 was caused by its protein
239 degradation using the proteasome inhibitor MG132. Upon MG132 treatment, ErbB2 protein
240 expression remained unchanged (Fig. 5G, H). This observation indicated that CDK4i disrupts
241 the interaction between Hsp90 and ErbB2, triggering ErbB2 degradation (Fig. S5L). To
242 confirm this, we treated cells with the Hsp90 inhibitor geldanamycin at a concentration that

243 suppressed ErbB2 expression by 40%, similar to the effect of CDK4i (Fig. S5M, N). As a
244 result, cell cycle progression grounded to a halt, and there was no substantial delay in the
245 G1/S transition (Movie S1). Therefore, the loss of ErbB2 protein stability following CDK4i
246 treatment may impair the regulation of c-Myc-mediated G1/S transition, even if c-Myc is
247 activated by epigenetic modification, thereby delaying the G1/S transition (Fig. 5I).

248 **High ErbB2 expression induces cell cycle arrest by repressing cyclin D1 activity via c-**
249 **Myc under CDK4 inhibition**

250 We speculated that ErbB2 protein instability contributes to the delay in G1/S entry under
251 CDK4i and thus could be counteracted by ErbB2 overexpression. To test this hypothesis, we
252 generated MCF-7 cells expressing varying levels of ErbB2, from moderate to high (Fig. S5A,
253 B), and analyzed their cell cycle phase distribution using live-cell imaging (Fig. 5J).
254 After CDK4i treatment, the proportion of S/G2/M-phase cells with high ErbB2 expression
255 was significantly reduced (OE-Moderate: 14.9%, OE-High: 12.5%; Fig. 5K), indicating cell
256 cycle arrest. We examined the protein expression of cyclin D1 and p-RB, which are critical
257 for initiating cell cycle entry (Fig. 5A, B). We observed a significant reduction in both cyclin
258 D1 and p-RB levels. Therefore, we investigated the cause of the decreased cyclin D1 levels.
259 The p27 protein reportedly promotes the assembly of the cyclin D1/CDK4 complex in the G1
260 phase (*34*), while its gene expression is inhibited by p-AKT and c-Myc (*35*). Our data
261 revealed that p27 protein expression decreased after CDK4i treatment, whereas p-AKT and c-
262 Myc protein levels tended to increase post treatment. By contrast, p-ERK levels remained
263 unchanged under different conditions. These findings suggested that, in ErbB2-
264 overexpressing cells, the enhanced p-AKT–c-Myc axis antagonizes the protein expression of
265 p27 and cyclin D1, leading to cell cycle arrest in the absence of CDK4 activity.

266 **Reversible cell cycle arrest is maintained by c-Myc transcriptional activity**

267 Drug resistance is closely linked to a reversible cell cycle arrest state regulated by residual

268 survival signals (*11*). In ErbB2-overexpressing cells, a cell cycle arrest state is induced after
269 CDK4 inhibition, but this may be reversed by the survival signals from c-Myc. In CDK4i-
270 treated cells with high ErbB2 expression, CDK4i removal increased cyclin D1, p27, and p-
271 RB levels, while c-Myc expression remained unchanged (Fig. 6A, B). We analyzed the c-
272 Myc phosphorylation (Ser^{62}) levels to confirm its elevated transcriptional activity in cell
273 cycle arrested cells. Single-cell analysis revealed that CDK4i depletion decreased the ratio of
274 phosphorylated c-Myc (Ser^{62}) to cyclin D1 (p-c-Myc/cyclin D1) and increased the ratio of S-
275 phase cells from 18.7% to 47.5% (Fig. 6C). ErbB2-overexpressing cells maintained a higher
276 p-c-Myc/cyclin D1 ratio than wild-type cells (Fig. S6A), suggesting that sustained cell cycle
277 arrest may result from persistent c-Myc transcriptional activation.
278 To investigate whether blocking c-Myc transcriptional activity could prevent reversible cell
279 cycle arrest, we treated cells with EN4 and CDK4i for 8 h, washed the inhibitors, and
280 analyzed cell cycle distribution at 52 h (72 h after HRG stimulation; Fig. 6D, E). The
281 combined treatment increased G1-phase and reduced S/G2/M-phase cell numbers, indicating
282 impaired cell cycle re-entry. CDK4i reduced p27 (*CDKN1B*) mRNA levels, which were
283 restored by co-treatment with EN4 (Fig. 6F, G), suggesting direct c-Myc regulation of p27
284 gene expression. Overall, these data supported the hypothesis that, in cells overexpressing
285 ErbB2, CDK4 inhibition promotes reversible cell cycle arrest due to an excessive increase in
286 c-Myc transcriptional activity and rapid decrease in cyclin D1 protein expression, which is
287 attributed to the reduction in p27 gene and protein expression.
288 Given the association between stable cell cycle arrest and cellular (*51*, *52*) or ErbB2-induced
289 senescence (*53*), we examined the senescence phenotype. Senescence associated β-
290 galactosidase (SA-β-Gal) staining intensity after 6 d of CDK4i treatment showed an inverse
291 correlation with ErbB2 expression. EN4 (4 μM) enhanced SA-β-Gal staining in WT MCF-7
292 cells beyond the effect of CDK4i alone but showed no additional effect in T47D or high

293 ErbB2-expressing MCF-7 cells (Fig. 6H, I). This finding was consistent with cell line-
294 specific sensitivity, since 2 nM EN4 induced cell cycle arrest in WT MCF-7 cells, whereas 2
295 μM was required for WT T47D cells (Fig. 4E, F). Our results suggested that ErbB2 levels
296 modulate the irreversibility of the G1/S transition under CDK4i treatment, and the addition of
297 a c-Myc inhibitor supports the irreversible state (Fig. 6J).
298

299 **Discussion**

300 Our findings reveal that ErbB2 receptor levels modulate the relative roles of cyclin D1 and c-
301 Myc in the G1/S transition, ultimately providing two distinct pathways for cell cycle
302 progression or arrest in the presence of CDK4i.
303 The luminal A subtype accounts for 30% of breast cancer cases. Although these patients
304 typically receive standard hormone therapy, CDK4/6is are also commonly used in cases of
305 more advanced or metastatic tumors (*5*, *54*). However, their success is limited by
306 heterogeneous drug responses. Notably, an ErbB2-overexpressing subpopulation has been
307 identified within luminal A breast cancer cells, which were initially characterized by low
308 ErbB2 expression (*55*). Given that these subpopulations occur relatively infrequently, at
309 approximately 7% of the total population (*56*), identifying differences in cell cycle regulation,
310 especially in terms of ErbB2 expression, is critical for improving cancer treatment. Long-
311 term CDK4i treatment, commonly used for luminal A breast cancer, activates alternative
312 pathways, such as PI3K/AKT/mTOR, androgen receptor, and Hippo signaling (*13*, *14*, *16*,
313 *17*), along with transcriptional reprogramming via non-coding RNAs (*15*, *57*), promoting the
314 development of drug resistance. To mitigate this resistance, pathways that may act at the very
315 early step of cell cycle entry must be inhibited. Accordingly, we investigated how ErbB2
316 levels within cells of the same luminal A subtype affect the core cell cycle regulatory network
317 and CDK4 inhibitor sensitivity (Fig. 7A, B). In MCF-7 cells under HRG stimulation, CDK4

318 RNA levels increased and remained elevated through R-point and S-phase entry, whereas
319 CDK6 RNA levels were quite low compared to those of CDK4 and tended to decrease after
320 HRG stimulation (Fig. S4D). Therefore, we focused on the effect of CDK4 inhibitors rather
321 than CDK4/6 inhibitors.
322 The temporal dynamics of the cell cycle regulators and live-cell imaging analysis showed that
323 the roles of cyclin D1 and c-Myc, key regulators of the G1/S transition, vary depending on
324 the expression status of ErbB2 under CDK4i treatment. This variation ultimately affects the
325 timing and irreversibility of the G1/S transition. In MCF-7 cells, a representative luminal A
326 breast cancer cell line with low ErbB2 expression, the G1/S transition is normally regulated
327 by the cyclin D1/CDK4 complex via Hsp90 (Fig. 5C–E; Fig. S5C–O). Although CDK
328 inhibitors are known to sequester Hsp90 and CDK4/6 (*58*), our results suggested that the
329 function of Hsp90 is complemented by CDK4 activity and contributes to stabilizing the
330 ErbB2 protein. This positive feedback mechanism provides valuable insights into the signal-
331 dependent complexity of cell cycle regulation. In the non-responsive subpopulations to
332 CDK4 inhibition, the G1/S transition persists, but with delays due to epigenetic modification
333 and increased c-Myc transcriptional activity and ErbB2 degradation (Fig. 4; Fig. 7A).
334 However, the excessive transcriptional activity of c-Myc promotes cell cycle arrest (Fig. 6A–
335 G) by rapidly reducing cyclin D1 and p27 levels. The expression of p27, which recruits
336 cyclin D1 to the nucleus during the G1 phase, is also repressed by AKT and c-Myc (*35*).
337 Therefore, in high ErbB2-expressing MCF-7 cells, with high levels of AKT and c-Myc
338 activity, CDK4 inhibition increases free cyclin D1 levels, rendering it more susceptible to
339 degradation (*59–61*). This process generates a hypophosphorylated RB state in ErbB2-
340 overexpressing MCF-7 cells compared to WT cells, leading to cell cycle arrest due to a
341 decrease in free E2F now bound to c-Myc (Fig. 7B).
342 c-Myc regulates the cell survival pathway (*35*, *62*). In ErbB2-overexpressing MCF-7 cells,

343 cell cycle arrest was reversible after CDK4 inhibition (Fig. 6D, E), suggesting that the
344 transcriptional activity of c-Myc promotes sustained cell survival in this context. Co-
345 treatment with inhibitors targeting the transcriptional activity of c-Myc and CDK4 may be
346 necessary to induce irreversible cell cycle arrest (Fig. 6H, I). However, at the same
347 concentration at which the Myc inhibitor promoted cellular senescence in WT MCF-7 cells,
348 the percentage of senescent WT T47D and ErbB2-overexpressing cells did not change
349 compared to that in the respective control conditions. For drug response assessments, the
350 threshold at which c-Myc switches from supporting cell survival to inducing irreversible cell
351 cycle arrest in relation to ErbB2 levels could inform the development of more effective
352 molecular-targeted treatment strategies for breast cancer.
353 Overall, our results suggest that the c-Myc-to-cyclin D1 ratio provides valuable quantitative
354 insights into the varying sensitivity of cancer cells to CDK4is, without relying solely on
355 observable cell proliferation rates or single biomarker gene analysis.
356

357 **Materials and methods**

358 **Reagents**

359 The MEKi PD0325901 was purchased from FUJIFILM Wako Pure Chemical Corp. (Osaka,
360 Japan); CDK4i V was purchased from Calbiochem (San Diego, CA, USA); AKTi VIII was
361 purchased from Cayman Chemical (Ann Arbor, MI, USA); EN4 (Myci) was purchased from
362 Selleck Chemicals (Houston, TX, USA); geldanamycin was purchased from FUJIFILM
363 Wako Pure Chemical Corp.; blasticidin was purchased from Kaken Pharmaceutical (Tokyo,
364 Japan); Lipofectamine LTX was purchased from Thermo Fisher Scientific (Waltham, MA,
365 USA); and HRG was procured from R&D Systems (Minneapolis, MN, USA).

366 **ErbB2 overexpression**

367 MCF-7 (ATCC, HTB-22) cells overexpressing full-length human ErbB2 (HER2) were

368 established as follows: Human ErbB2 cDNA in the pCMV6-XL5 vector was purchased from
369 OriGene (Catalog No: TC128161, Rockville, MD, USA). The cDNA fragment was cloned
370 into the vector pCMV-6-Neo vector (OriGene). The plasmid was then transfected into MCF-7
371 cells using Lipofectamine LTX (Invitrogen, Carlsbad, CA, USA) according to the
372 manufacturer's protocol, and stable transfectants were selected with G418 (neomycin).
373 Colonies derived from single cells compartmentalized in 96-well plates were isolated and
374 examined. ErbB2 expression was examined via western blotting to group cells with moderate
375 or high ErbB2 expression (as described below for protein extraction and immunoblotting).

376 **Cell culture**

377 MCF-7, ErbB2-overexpressing MCF-7, and T47D (ATCC, HTB-133) cells were cultured in
378 Dulbecco's modified Eagle's medium (DMEM, Nacalai Tesque, Kyoto, Japan) supplemented
379 with 10% (*v/v*) fetal bovine serum (FBS, Sigma-Aldrich, Saint Louis, MO, USA) and 1%
380 penicillin–streptomycin (100 IU/ml penicillin, 100 μg/ml streptomycin; Nacalai Tesque) at
381 37 °C in a humidified 5%-CO_2 atmosphere. Cells were routinely tested using a CycleavePCR
382 Mycoplasma Detection Kit (Takara bio, CY-232); no mycoplasma contamination was
383 detected.

384 **FUCCI transfection**

385 MCF-7 and ErbB2-overexpressing MCF-7 cells stably expressing the FUCCI biosensor were
386 generated using a PiggyBac transposase system (*63*). Lipofectamine LTX (Thermo Fisher
387 Scientific) was used to transfect the FUCCI plasmid (pPBbsr2-H2B-iRFP-P2A-mScarlet-I-
388 hGem-P2A-PIP-tag-NLS-mNeonGreen; https://benchling.com/s/seq-
389 LPZ1tLdpgnpJIYOG2ujR) along with hyPBase (https://benchling.com/s/seq-
390 oGkw53b41IZqvzF5yQ9K) into MCF-7 and ErbB2-overexpressing MCF-7 cells, following
391 the manufacturer's protocol (*64*). Cells were suspended in a drug-free medium for 48 h and
392 treated with blasticidin (10 μg/ml) to separate those stably expressing the plasmid. Colonies

393 derived from single cells compartmentalized in 96-well plates were selected by microscopic
394 live-cell observation of Geminin and PIP-tag fluorescence.

395 **Protein extraction and immunoblotting**

396 MCF-7, T47D, and ErbB2-overexpressing (moderate or high) MCF-7 cells were seeded in
397 six-well plates (450 000 cells/well) and cultured in 10% FBS containing DMEM for 48 h. The
398 medium was changed to FBS-free phenol red-free DMEM (FUJIFILM Wako Pure Chemical
399 Corp.) containing 1% penicillin–streptomycin (100 IU/ml penicillin, 100 μg/ml streptomycin;
400 Nacalai Tesque) and 1% 100 mmol/L sodium pyruvate solution (FUJIFILM Wako Pure
401 Chemical Corp.), and the cells were cultured for 17 h. The medium was changed again, and
402 the cells were cultured for 3 h. After administration of 10 nM HRG (R&D Systems) for 12 h,
403 the cells were independently treated with CDK4i and dimethyl sulfoxide (DMSO). Serum
404 was not included under conditions where HRG was added. Total cell lysates were prepared in
405 RIPA buffer (Nacalai Tesque, 1648834) containing protease inhibitors (11836153001, Roche
406 Rotkreuz, Switzerland) and phosphatase inhibitors (Roche, 4906837001) at 4 °C. Cells were
407 vortexed for 5 min and centrifuged at 16 000 × *g* and 4 °C for 15 min. The supernatant was
408 collected and denatured by heating at 95 °C with sample buffer (5×) and 2-mercaptoethanol
409 (Nacalai Tesque, 21418-55) for 5 min. The proteins were subjected to SDS polyacrylamide
410 gel electrophoresis (Nacalai Tesque, 1306644), transferred to polyvinylidene fluoride
411 membranes (Merck, Darmstadt, Germany), and incubated with 10% blocking buffer (Nacalai
412 Tesque, 03953-95) prepared in Tris-buffered saline/Tween 20 (TBS-T; T9142; Takara Bio,
413 Shiga, Japan) for 1 h at 25 °C. Membranes were probed overnight with antibodies against
414 AKT (1:1 000; #4685; Cell Signaling Technology, Danvers, MA, USA), p-AKT (Thr^{308}; 1:1
415 000; Cell Signaling Technology; #2965), ERK (1:1 000; Cell Signaling Technology; #9102),
416 p-ERK (Thr^{202} Tyr^{204}; 1:1 000; Cell Signaling Technology; #4370), HER2/ErbB2 (1:1 000;
417 Cell Signaling Technology; #2165), p-HER2/ErbB2 ($Thr^{1221/1222}$; 1:1 000; Cell Signaling

418 Technology; #2249), p-c-Fos (Ser^{374}; 1:1 000; #ab55836; Abcam, Cambridge, UK), c-Fos
419 (1:200; #sc-166940; Santa Cruz Biotechnology, Dallas, TX, USA), p-c-Myc (Ser^{62}; 1:1 000;
420 Abcam; #ab51156), c-Myc (1:200; Santa Cruz; #sc-40), E2F-1 (1:1 000; Cell Signaling
421 Technology; #3742), p-RB (Ser$^{807/811}$; 1:1 000; Cell Signaling Technology; #8516), p-RB
422 (Thr^{373}; 1:1 000; Abcam; #ab52975), RB1 (1:1 000; #SPM353; NOVUS biologicals,
423 Centennial, CO, USA), cyclin D1 (1:1 000; Cell Signaling Technology; #2978), cyclin E
424 (1:200; Santa Cruz; #sc-247), cyclin A (1:200; Santa Cruz; #sc-271682), CDK4 (1:1 000;
425 Santa Cruz; #DSC-35), CDK2 (1:1 000; Santa Cruz; #D-12), P27 Kip1 (1:1 000; Cell
426 Signaling Technology; #3686), and GAPDH (1:4 000; 10494-1-AP; Proteintech, Boston, MA,
427 USA) in TBS-T including 10% blocking buffer at 4 °C. They were then incubated with
428 horseradish peroxidase (HRP)-conjugated secondary antibodies, HRP-conjugated anti-mouse
429 IgG (1:5000; Cell Signaling Technology; #7076) and HRP-conjugated anti-rabbit IgG
430 (1:5000; Cell Signaling Technology; #7074), for 1 h at room temperature. The membranes
431 were developed using a chemiluminescent HRP substrate (Merck). Protein bands were
432 detected using an Amersham Imager 600 UV (GE Healthcare, Eindhoven, Netherlands) and
433 visualized using the ImageJ-Fiji software (v.2.14.0/1.54f, NIH, Bethesda, MD, USA).
434 **qRT-PCR**
435 qRT-PCR was conducted as previously described (*65*). RNA was isolated from cells using
436 NucleoSpin RNA Plus (Cat. No. 740984.250; Macherey-Nagel, Duren, Germany) according
437 to the manufacturer's protocol. cDNA was synthesized using ReverTra Ace qPCR RT Master
438 Mix (TOYOBO, Osaka, Japan), and quantitative PCR was performed using a KOD SYBR
439 qPCR kit (TOYOBO) on a CFX96 Real-Time PCR System (Bio-Rad Laboratories, Hercules,
440 CA, USA). The ΔΔCq method was used to quantify gene expression, using *RPL27*
441 expression as an internal reference (*66*). The primers used for real-time PCR are listed in
442 Table S1.

443 **Cell cycle analysis using the FUCCI biosensor**

444 Cell cycle analysis was conducted as previously described (*65*). Time-lapse microscopy was
445 performed using an IN Cell Analyzer 2500HS (GE Healthcare, Chicago, IL, USA) equipped
446 with a CFI S Plan Fluor ELWD dry objective lens 20× (NA: 0.45) at an excitation
447 wavelength of 475 nm and emission wavelength of 511 nm for PIP-tag-mNeonGreen, and an
448 excitation wavelength of 542 nm and emission wavelength of 597 nm for mScarlet-hGem.
449 Cells were maintained at 37 °C in a humidified 5%-CO_2 atmosphere and imaged at 20-min
450 intervals for 72 h. Image processing and quantification of cell cycle phase distribution were
451 performed using ImageJ-Fiji software (v.2.14.0/1.54f, NIH). Masks of the mScarlet-hGem
452 and PIP-tag-mNeonGreen signals were obtained by applying a fixed threshold using
453 "Analyze Particles" and automatically counted as ROIs. Cell cycle phases were determined in
454 the following manner: G1 phase, PIP-tag-positive; S phase, hGem-positive; G2/M phase,
455 PIP-tag- and hGem-positive. The average brightness of mScarlet and mNeonGreen was
456 obtained using cell-tracking software (Olympus, Tokyo, Japan). The threshold parameters for
457 mScarlet and mNeonGreen were set manually for each cell line. We employed an algorithm
458 for estimating the cell cycle phase at the single-cell level using R packages [brunnermunzel
459 (v.1.4.1), multimode (v.1.4), rlist (v.0.4.6.1), and tidyverse (v.1.3.0)]. The duration of each
460 cell cycle phase was obtained from the single-cell data.

461 **Nucleus count**

462 The number of nuclei was quantified based on the fluorescence of the FUCCI probes, and
463 signals for a nuclear marker (histone H2B), mScarlet-hGem, and PIP-tag-mNeonGreen were
464 used to determine cell proliferation. Image processing and nuclear ratio quantification were
465 performed using the ImageJ-Fiji software (v.2.14.0/1.54f, NIH). Masks of the merged nuclear
466 marker, mScarlet-hGem, and PIP-tag-mNeonGreen signals were obtained by applying a fixed
467 threshold using "Analyze Particles" and automatically counted as ROIs. The nuclear ratio

468 was calculated by dividing the number of nuclei at the end of observation by that at the
469 beginning. Thus, a nuclear ratio near 1.0 indicated potential cell cycle arrest, above 1.0
470 indicated cell proliferation, and below 1.0 indicated apoptosis.

471 **Immunostaining and quantitative analysis of images**

472 MCF-7 and ErbB2-overexpressing (moderate or high) cells were seeded in 12-well plates
473 (200 000 cells/well) and cultured in 10% FBS containing DMEM for 48 h. The medium was
474 changed to FBS-free phenol red-free DMEM (FUJIFILM Wako Pure Chemical Corp.)
475 containing 1% penicillin–streptomycin (100 IU/ml penicillin, 100 μg/ml streptomycin;
476 Nacalai Tesque) and 1% 100 mmol/L sodium pyruvate solution (FUJIFILM Wako Pure
477 Chemical Corp.), and the cells were cultured for 17 h. The medium was changed again, and
478 the cells were cultured for 3 h. After administration of 10 nM HRG (R&D Systems) for 12 h,
479 the cells were independently treated with CDK4i and DMSO. Serum was not included under
480 conditions where HRG was added. Cells were washed twice with PBS at the indicated times,
481 fixed for 2 min with pre-prepared methanol at –20 °C, washed twice with Blocking One
482 (Nacalai Tesque, 03953-95), and incubated overnight at 4 °C with Blocking One. The next
483 day, cells were incubated overnight at 4 °C with primary antibodies diluted in 10% goat
484 serum (Thermo Fisher Scientific, 16210064)/Blocking One, washed five times with PBS, and
485 incubated with fluorescent dye-conjugated secondary antibody, 2 μg/ml DAPI (Nacalai
486 Tesque, 11034-56), and 0.5 μg/ml CellMask (Thermo Fisher Scientific, H32721) for 1 h at
487 room temperature. Cells were washed five times with PBS, and images were acquired using
488 the IN Cell Analyzer 2500HS (GE Healthcare Life Science) at 20× magnification. At least
489 three images were collected for each treatment, containing at least 100 cells each, for
490 quantification using the ImageJ-Fiji software (v.2.14.0/1.54f, NIH) and CellProfiler (v.4.2.1).
491 Co-localization analysis for Hsp90 with either ErbB2 or PY100 was performed using the
492 "Coloc 2" plugin in the ImageJ-Fiji software. Cell fractionation was performed on CellMask-

493 stained images using CellProfiler, and the mean intensity was calculated for p-c-Myc, cyclin
494 D1, and DAPI in each cell. The ratio of phosphorylated c-Myc (Ser^{62}) to cyclin D1 (p-c-
495 Myc/cyclin D1) for each cell was plotted over the DAPI intensity. The DAPI intensity
496 indicating the G1/S transition was determined based on the percentage of cells that were in
497 the S/G2 /M phase 24 h after HRG stimulation. In WT MCF-7 cells, 22.4% of cells were in
498 the S/G2/M phase, at which time the DAPI intensity was 0.105. In MCF-7 cells
499 overexpressing ErbB2 (high), 25.4% of the cells were in the S/G2/M phase, at which time the
500 DAPI intensity was 0.0775.

501 **Analysis of senescence associated β-galactosidase-positive cells**

502 SA-b-gal staining was conducted as previously described (*65*). Briefly, senescent cells were
503 stained using a Senescence β-Galactosidase Staining Kit (#9860; Cell Signaling Technology)
504 according to the manufacturer's instructions. Images were acquired with a BZ-9000
505 microscope (Keyence, Osaka, Japan) at 20× magnification. The percentage of SA-β-gal-
506 positive cells was calculated from images using CellProfiler (v.4.2.1). The total number of
507 cells was determined by visualizing nuclear segmentation with DAPI staining. The number of
508 SA-β-gal-stained cells was identified using the UnmixColors module. The percentage of SA-
509 β-gal-positive cells was calculated by dividing the number of SA-β-gal-stained cells by the
510 total number of nuclei in each field of view.

511 **RNA-seq**

512 FUCCI-expressing MCF-7 cells were seeded in six-well plates (450 000 cells/well) and
513 cultured in 10% FBS containing DMEM for 48 h. The medium was changed to FBS-free
514 phenol red-free DMEM, the cells were cultured for 17 h, the medium was changed again, and
515 the cells were cultured for 3 h. After administration of 10 nM HRG for 12 h, the cells were
516 independently treated with CDK4i and DMSO. Serum was not included under conditions
517 where HRG was added. Cells were washed twice with PBS at the indicated times. Total RNA

518 was isolated using NucleoSpin RNA Plus (Macherey-Nagel; Cat. No. 740984.250) at the
519 specified time. Library construction and RNA-seq were performed on an Illumina sequencing
520 platform (Rhelixa Tokyo, Japan). Poly(A) RNA was prepared with a Poly(A) mRNA
521 Magnetic Isolation Module (E7490; New England Biolabs, Ipswich, MA, USA), and the
522 sequencing library was generated using a NEBNext Ultra II Directional RNA Library Prep
523 Kit (New England Biolabs, E7760). RNA-seq was performed on a NovaSeq 6000 (Illumina,
524 San Diego, CA, USA) with 150-bp paired-end reads. Raw reads were quality-checked using
525 FastQC (v.0.11.9) and trimmed using TrimGalore (v.0.6.0) (*67*). Trimmed reads were mapped
526 using STAR (v.2.7.9a) (*68*) with GRCh38 as the reference genome. featureCounts (v.1.6.4)
527 (*69*) was used to construct the count matrix with the "-p -B -t exon -g gene_name"
528 parameters. Raw counts were converted to transcripts per kilobase million and corrected
529 using EdgeR (v.3.36.0) (*70*). Principal component analysis was performed using the prcomp
530 function in R (v.4.1.1) (*71*). GSEA was performed using the fgsea package (v.1.20.0) (*72*) and
531 the hallmark gene set in the Human MSigDB Collections (*49*).

532 **ChIP-seq**

533 FUCCI-expressing MCF-7 cells were seeded in 100-mm dishes (2 300 000 cells/dish) and
534 cultured in 10% FBS containing DMEM for 48 h. The medium was changed to FBS-free
535 phenol red-free DMEM, the cells were cultured for 17 h, the medium was changed, and the
536 cells were cultured for 3 h. After administration of 10 nM HRG for 12 h, the cells were
537 independently treated with CDK4i and DMSO. Cells were washed twice with PBS at the
538 indicated times. Cells were fixed with 1% formaldehyde (Thermo Fisher Scientific) for 5
539 min. Fragmented DNA was obtained using a SimpleChIP Plus Enzymatic Chromatin IP Kit
540 (Cell Signaling Technology, 9005) and M220 Focused-ultrasonicator (Covaris, Woburn, MA,
541 USA). Immunoprecipitated DNA was obtained using an Auto iDeal ChIP-seq kit for Histones
542 ×24 (Diagenode, Liege, Belgium) on an SX-8G platform (Diagenode). Next, 2 μg anti-

543 H3K27Ac antibody (Diagenode) and 2 μg anti-H3K4me1 antibody (Diagenode) were mixed
544 with 10 μl DiaMag Protein A-coated magnetic beads, and IP reactions with DNA were
545 performed for 12 h. De-crosslinking was conducted using 4 μl of 5 M NaCl and 1 μl of 20
546 mg/ml proteinase K (Thermo Fisher Scientific) for 4 h at 60 °C. Library construction and
547 RNA-seq were performed using the Illumina sequencing platform (Rhelixa). A sequencing
548 library was generated using a NEBNext Ultra II DNA Library Prep Kit for Illumina (New
549 England Biolabs, 7645). ChIP-seq was performed on the NovaSeq 6000 (Illumina) with 150-
550 bp paired-end reads. H3K27Ac ChIP-seq and H3K4me1 data were processed using the same
551 protocol as for RNA-seq. FastQC (v.0.11.9) was used for quality control. Trimming was
552 performed using Trimmomatic (v.0.39) (*73*) with the following parameters:
553 ILLUMINACLIP, TruSeq2-SE; fa, 2:30:10; LEADING, 30; TRAILING, 30;
554 SLIDINGWINDOW, 4:15; MINLEN, 30; HEADCROP, 2. Reads were mapped using
555 Bowtie2 (v.2.4.4) (*74*) with GRCh38 as the reference genome, and duplicate reads were
556 excluded using Picard (v.2.26.6) (*75*). Bigwig files were created from the generated BAM
557 files using deepTools (v.3.5.1; bamCoverage function) (*76*). Peak regions were identified
558 using HOMER (v.4.11) (*77*) with the "-style histone -L 0 -fdr 0.00005" parameters. All
559 detected peak regions were annotated to their nearest neighbor genes using HOMER
560 annotatePeaks.pl (v.4.11).

561 **Promoter and enhancer detection**

562 Promoter regions were defined as those in the H3K27Ac peak that did not overlap with the
563 H3K4me1 peak and were within 250-bp of the transcription start site (TSS, at the center of
564 the peak). Enhancer regions were defined as those in the H3K27Ac peak overlapping with the
565 H3K4me1 peak and were more than 250-bp from the TSS. The TSS was obtained from the
566 Ensembl database using BiomaRt (v.2.50.3) (*78*). The bed files containing the promoter and
567 enhancer regions for all time points were merged, and the time-course of the coverage values

568 for H3K27Ac ChIP-seq was calculated using HOMER annotatePeaks.pl (v.4.11). The
569 estimated coverage values were used to detect promoters and enhancers affected by CDK4i.
570 Promoters that gained or lost signal were defined as those with coverage values of $|\log_2 FC| >$
571 0.3 for inhibitor and control conditions. Enhancers that gained or lost signals were defined as
572 those with coverage values changing by $|\log_2 FC| > 0.3$ and target gene expression changing
573 by $|\log_2 FC| > 0.2$ in the same direction as the change in enhancer activity.

574 **Motif analysis of ChIP-seq data**

575 Motif analysis was performed using MEME Suite SEA (v.5.4.1) (*79*). The motif files were
576 obtained from the JASPAR 2022 database
577 (JASPAR2022_CORE_vertebrates_nonredundant_v2) (*80*). Peak regions containing motifs
578 were detected using MEME Suite FIMO (v.5.4.1). The analysis was performed using default
579 parameters.

580 **Transcription factor enrichment analysis**

581 Transcription factor analysis was conducted using DoRothEA (v.1.6.0) (*42*) with the
582 "run_viper" function. We used regulon data with "confidence" levels of A and B. Target genes
583 were selected based on their changes in expression (FDR < 0.01) between the control and
584 inhibitor treatments at each time point.

585 **Clinical data analysis**

586 We used microarray gene expression data (GEO GSE93204) for biopsy samples from the
587 NeoPalAna clinical trial (NCT01723774) (*50*) to identify differentially expressed genes based
588 on *P*-values adjusted using the Benjamini–Hochberg method to control the false discovery
589 rate in GEO2R.

590 **Statistical analysis**

591 Statistical analysis, data visualization, and Kolmogorov–Smirnov normality testing were
592 performed in the R software (v.4.2.1; The R Foundation, Vienna, Austria). For normally

distributed data, the Student's *t*-test and Welch's two-sample *t*-test were used after confirming equal variances using the F-test for comparisons between two groups. Comparisons between more than two groups were performed using one-way analysis of variance followed by the Tukey's post-hoc test. For non-normally distributed data, a Kruskal–Wallis test or Mann–Whitney U test was used. $P < 0.05$ was considered significant.

Acknowledgments:

We thank all members of the Laboratory for Cell Systems at the Institute for Protein Research for the discussions regarding our research and especially Mr. Kyoichi Ebata for helping to design the cell cycle analysis. We also thank Mr. Hideya Aragaki from Olympus Corporation for providing the cell-tracking software.

Funding:

JSPS KAKENHI (18H04031, MO; 21K15503, ANI)

JST CREST Program (JPMJCR21N3, MO)

Uehara Memorial Foundation (MO)

Kaneko Narita Research Grant from the Protein Research Foundation (ANI)

New Field Development Support Program from the Institute for Protein Research (ANI)

Joint Research Grant from ExCELLS (MO, KA)

Contributions:

Conceptualization: ANI, MO

Methodology: ANI, KM, KA, MO

Validation: ANI

Formal analysis: ANI, KM

618 Investigation: ANI, KM

619 Resources: ANI, KA, MO

620 Visualization: ANI, KM

621 Writing – Original Draft: ANI, KM, MO

622 Writing – Review & Editing: ANI, KM, KA, MO

623 Supervision: ANI, MO

624 Project administration: ANI, MO

625 Funding acquisition: ANI, KA, MO

626

627 **Data availability:** The sequence data for RNA-seq and ChIP-seq reported in this paper have
628 been deposited in the DNA Data Bank of Japan with accession number ESUB001718. The
629 code is available at https://github.com/okadalabipr/HER2_Cellcycle. All other data will be
630 made available upon reasonable request.

631

632 **References**

633 1. Zetterberg A, Larsson O. Kinetic analysis of regulatory events in G1 leading to
634 proliferation or quiescence of Swiss 3T3 cells. Proc Natl Acad Sci U S A. 1985; 82:
635 5365–5369.

636 2. Rubin SM, Sage J, Skotheim JM. Integrating old and new paradigms of G1/S control.
637 Mol Cell. 2020; 80: 183–192.

638 3. Matthews HK, Bertoli C, de Bruin RAM. Cell cycle control in cancer. Nat Rev Mol Cell
639 Biol. 2022; 23: 74–88.

640 4. Yu Q, Geng Y, Sicinski P. Specific protection against breast cancers by cyclin D1
641 ablation. Nature. 2001; 411: 1017–1021.

642 5. Adon T, Shanmugarajan D, Kumar HY. CDK4/6 inhibitors: A brief overview and

643 prospective research directions. RSC Adv. 2021; 11: 29227–29246.
644 6. Asghar U, Witkiewicz AK, Turner NC, Knudsen ES. The history and future of targeting
645 cyclin-dependent kinases in cancer therapy. Nat Rev Drug Discov. 2015; 14: 130–146.
646 7. Weigelt B, Peterse JL, van, van 't Veer LJ.. Breast cancer metastasis: Markers and
647 models. Nat Rev Cancer. 2005; 5: 591–602.
648 8. Perou CM, Sørlie T, Eisen MB, van de Rijn M, Jeffrey SS, Rees CA, et al. Molecular
649 portraits of human breast tumours. Nature. 2000; 406: 747–752.
650 9. Sørlie T, Perou CM, Tibshirani R, Aas T, Geisler S, Johnsen H, et al. Gene expression
651 patterns of breast carcinomas distinguish tumor subclasses with clinical implications.
652 Proc Natl Acad Sci U S A. 2001; 98: 10869–10874.
653 10. Finn RS, Dering J, Conklin D, Kalous O, Cohen DJ, Desai AJ, et al. PD 0332991, a
654 selective cyclin D kinase 4/6 inhibitor, preferentially inhibits proliferation of luminal
655 estrogen receptor-positive human breast cancer cell lines in vitro. Breast Cancer Res.
656 2009; 11: R77.
657 11. Lüönd F, Tiede S, Christofori G. Breast cancer as an example of tumour heterogeneity
658 and tumour cell plasticity during malignant progression. Br J Cancer. 2021; 125: 164–
659 175.
660 12. McGranahan N, Swanton C. Clonal heterogeneity and tumor evolution: Past, present,
661 and the future. Cell. 2017; 168: 613–628.
662 13. Herrera-Abreu MT, Palafox M, Asghar U, Rivas MA, Cutts RJ, Garcia-Murillas I, et al.
663 Early adaptation and acquired resistance to CDK4/6 inhibition in estrogen receptor–
664 positive breast cancer. Cancer Res. 2016; 76: 2301–2313.
665 14. Knudsen ES, Kumarasamy V, Ruiz A, Sivinski J, Chung S, Grant A, et al. Cell cycle
666 plasticity driven by mTOR signaling: Integral resistance to CDK4/6 inhibition in
667 patient-derived models of pancreatic cancer. Oncogene. 2019; 38: 3355–3370.

668 15. Cai Z, Shi Q, Li Y, Jin L, Li S, Wong LL, et al. LncRNA EILA promotes CDK4/6
669 inhibitor resistance in breast cancer by stabilizing cyclin E1 protein. Sci Adv. 2023; 9:
670 eadi3821.
671 16. Ji W, Shi Y, Wang X, He W, Tang L, Tian S, et al. Combined androgen receptor blockade
672 overcomes the resistance of breast cancer cells to palbociclib. Int J Biol Sci. 2019; 15:
673 522–532.
674 17. Li Z, Razavi P, Li Q, Toy W, Liu B, Ping C, et al. Loss of the FAT1 tumor suppressor
675 promotes resistance to CDK4/6 inhibitors via the Hippo pathway. Cancer Cell. 2018; 34:
676 893–905.e8.
677 18. Ross JS, Fletcher JA. The HER-2/neu oncogene in breast cancer: Prognostic factor,
678 predictive factor, and target for therapy. Oncologist. 1998; 3: 237–252.
679 19. Lenferink AE, Busse D, Flanagan WM, Yakes FM, Arteaga CL. ErbB2/neu kinase
680 modulates cellular p27(Kip1) and cyclin D1 through multiple signaling pathways.
681 Cancer Res. 2001; 61: 6583–6591.
682 20. Moasser MM. The oncogene HER2: Its signaling and transforming functions and its role
683 in human cancer pathogenesis. Oncogene. 2007; 26: 6469–6487.
684 21. Yarden Y, Sliwkowski MX. Untangling the ErbB signalling network. Nat Rev Mol Cell
685 Biol. 2001; 2: 127–137.
686 22. Nakakuki T, Birtwistle MR, Saeki Y, Yumoto N, Ide K, Nagashima T, et al. Ligand-
687 specific c-Fos expression emerges from the spatiotemporal control of ErbB network
688 dynamics. Cell. 2010; 141: 884–896.
689 23. Burch PM, Yuan Z, Loonen A, Heintz NH. An extracellular signal-regulated kinase 1-
690 and 2-dependent program of chromatin trafficking of c-Fos and Fra-1 is required for
691 cyclin D1 expression during cell cycle reentry. Mol Cell Biol. 2004; 24: 4696–4709.
692 24. Keller UB, Old JB, Dorsey FC, Nilsson JA, Nilsson L, MacLean KH, et al. Myc targets

693 Cks1 to provoke the suppression of p27^{Kip1}, proliferation and lymphomagenesis. EMBO
694 J. 2007; 26: 2562–2574.
695 25. Dong P, Maddali MV, Srimani JK, Thélot F, Nevins JR, Mathey-Prevot B, et al. Division
696 of labour between Myc and G1 cyclins in cell cycle commitment and pace control. Nat
697 Commun. 2014; 5: 4750.
698 26. Pardee AB. A restriction point for control of normal animal cell proliferation. Proc Natl
699 Acad Sci U S A. 1974; 71: 1286–1290.
700 27. Yao G, Tan C, West M, Nevins JR, You L. Origin of bistability underlying mammalian
701 cell cycle entry. Mol Syst Biol. 2011; 7: 485.
702 28. Spencer SL, Cappell SD, Tsai F-C, Overton KW, Wang CL, Meyer T. The proliferation-
703 quiescence decision is controlled by a bifurcation in CDK2 activity at mitotic exit. Cell.
704 2013; 155: 369–383.
705 29. Murphy LO, MacKeigan JP, Blenis J. A network of immediate early gene products
706 propagates subtle differences in mitogen-activated protein kinase signal amplitude and
707 duration. Mol Cell Biol. 2004; 24: 144–153.
708 30. Leone G, Sears R, Huang E, Rempel R, Nuckolls F, Park CH, et al. Myc requires
709 distinct E2F activities to induce S phase and apoptosis. Mol Cell. 2001; 8: 105–113.
710 31. Lee T, Yao G, Nevins J, You L. Sensing and integration of Erk and PI3K signals by Myc.
711 PLOS Comput Biol. 2008; 4: e1000013.
712 32. Chambard J-C, Lefloch R, Pouysségur J, Lenormand P. ERK implication in cell cycle
713 regulation. Biochim Biophys Acta. 2007; 1773: 1299–1310.
714 33. Muise-Helmericks RC, Grimes HL, Bellacosa A, Malstrom SE, Tsichlis PN, Rosen N.
715 Cyclin D expression is controlled post-transcriptionally via a phosphatidylinositol 3-
716 kinase/Akt-dependent pathway. J Biol Chem. 1998; 273: 29864–29872.
717 34. Larrea MD, Liang J, Da Silva T, Hong F, Shao SH, Han K, et al. Phosphorylation of

718 p27Kip1 regulates assembly and activation of cyclin D1-Cdk4. Mol Cell Biol. 2008; 28:
719 6462–6472.
720 35. García-Gutiérrez L, Delgado MD, León J. MYC oncogene contributions to release of
721 cell cycle brakes. Genes. 2019; 10: 244.
722 36. Nagashima T, Shimodaira H, Ide K, Nakakuki T, Tani Y, Takahashi K, et al. Quantitative
723 transcriptional control of ErbB receptor signaling undergoes graded to biphasic response
724 for cell differentiation. J Biol Chem. 2007; 282: 4045–4056.
725 37. Jeong H, Kim J, Lee Y, Seo JH, Hong SR, Kim A. Neuregulin-1 induces cancer stem
726 cell characteristics in breast cancer cell lines. Oncol Rep. 2014; 32: 1218–1224.
727 38. Grant GD, Kedziora KM, Limas JC, Cook JG, Purvis JE. Accurate delineation of cell
728 cycle phase transitions in living cells with PIP-FUCCI. Cell Cycle. 2018; 17: 2496–
729 2516.
730 39. Imoto H, Okada M. Signal-dependent regulation of early-response genes and cell cycle:
731 A quantitative view. Curr Opin Syst Biol. 2019; 15: 100–108.
732 40. Chung M, Liu C, Yang HW, Köberlin MS, Cappell SD, Meyer T. Transient hysteresis in
733 CDK4/6 activity underlies passage of the restriction point in G1. Mol Cell. 2019; 76:
734 562–573.e4.
735 41. Mueller S, Huard J, Waldow K, Huang X, D'Alessandro LA, Bohl S, et al. T160-
736 phosphorylated CDK2 defines threshold for HGF dependent proliferation in primary
737 hepatocytes. Mol Syst Biol. 2015; 11: 795.
738 42. Garcia-Alonso L, Holland CH, Ibrahim MM, Turei D, Saez-Rodriguez J. Corrigendum:
739 Benchmark and integration of resources for the estimation of human transcription factor
740 activities. Genome Res. 2021; 31: 745.
741 43. Joyce D, Albanese C, Steer J, Fu M, Bouzahzah B, Pestell RG. NF-κB and cell-cycle
742 regulation: The cyclin connection. Cytokine Growth Factor Rev. 2001; 12: 73–90.

743 44. Hirano T, Ishihara K, Hibi M. Roles of STAT3 in mediating the cell growth,
744 differentiation and survival signals relayed through the IL-6 family of cytokine
745 receptors. Oncogene. 2000; 19: 2548–2556.
746 45. Ernst J, Kheradpour P, Mikkelsen TS, Shoresh N, Ward LD, Epstein CB, et al. Mapping
747 and analysis of chromatin state dynamics in nine human cell types. Nature. 2011; 473:
748 43–49.
749 46. Road Map Epigenomics Consortium, Kundaje A, Meuleman W, Ernst J, Bilenky M, Yen
750 A, et al. Integrative analysis of 111 reference human epigenomes. Nature. 2015; 518:
751 317–330.
752 47. Liu Z, Venkatesh SS, Maley CC. Sequence space coverage, entropy of genomes and the
753 potential to detect non-human DNA in human samples. BMC Genomics. 2008; 9: 509.
754 48. Guo J, Li T, Schipper J, Nilson KA, Fordjour FK, Cooper JJ, et al. Sequence specificity
755 incompletely defines the genome-wide occupancy of Myc. Genome Biol. 2014; 15: 482.
756 49. Subramanian A, Tamayo P, Mootha VK, Mukherjee S, Ebert BL, Gillette MA, et al.
757 Gene set enrichment analysis: A knowledge-based approach for interpreting genome-
758 wide expression profiles. Proc Natl Acad Sci U S A. 2005; 102: 15545–15550.
759 50. Ma CX, Gao F, Luo J, Northfelt DW, Goetz M, Forero A, et al. NeoPalAna:
760 Neoadjuvant palbociclib, a cyclin-dependent kinase 4/6 inhibitor, and anastrozole for
761 clinical stage 2 or 3 estrogen receptor-positive breast cancer. Clin Cancer Res. 2017; 23:
762 4055–4065.
763 51. Gorgoulis V, Adams PD, Alimonti A, Bennett DC, Bischof O, Bishop C, et al. Cellular
764 senescence: Defining a path forward. Cell. 2019; 179: 813–827.
765 52. Huang W, Hickson LJ, Eirin A, Kirkland JL, Lerman LO. Cellular senescence: The
766 good, the bad and the unknown. Nat Rev Nephrol. 2022; 18: 611–627.
767 53. Trost TM, Lausch EU, Fees SA, Schmitt S, Enklaar T, Reutzel D, et al. Premature

768 senescence is a primary fail-safe mechanism of ERBB2-driven tumorigenesis in breast
769 carcinoma cells. Cancer Res. 2005; 65: 840–849.
770 54. Polk A, Kolmos IL, Kümler I, Nielsen DL. Specific CDK4/6 inhibition in breast cancer:
771 A systematic review of current clinical evidence. ESMO Open. 2016; 1: e000093.
772 55. Turner KM, Yeo SK, Holm TM, Shaughnessy E, Guan J-L. Heterogeneity within
773 molecular subtypes of breast cancer. Am J Physiol Cell Physiol. 2021; 321: C343–C354.
774 56. Prat A, Perou CM. Deconstructing the molecular portraits of breast cancer. Mol Oncol.
775 2011; 5: 5–23.
776 57. Ji W, Zhang W, Wang X, Shi Y, Yang F, Xie H, et al. c-myc regulates the sensitivity of
777 breast cancer cells to palbociclib via c-myc/miR-29b-3p/CDK6 axis. Cell Death Dis.
778 2020; 11: 760.
779 58. Hallett ST, Pastok MW, Morgan RML, Wittner A, Blundell KLIM, Felletar I, et al.
780 Differential regulation of G1 CDK complexes by the Hsp90-Cdc37 chaperone system.
781 Cell Rep. 2017; 21: 1386–1398.
782 59. Alao JP. The regulation of cyclin D1 degradation: Roles in cancer development and the
783 potential for therapeutic invention. Mol Cancer. 2007; 6: 24.
784 60. Guiley KZ, Stevenson JW, Lou K, Barkovich KJ, Kumarasamy V, Wijeratne TU, et al.
785 p27 allosterically activates cyclin-dependent kinase 4 and antagonizes palbociclib
786 inhibition. Science. 2019; 366: eaaw2106.
787 61. Sears R, Nuckolls F, Haura E, Taya Y, Tamai K, Nevins JR. Multiple Ras-dependent
788 phosphorylation pathways regulate Myc protein stability. Genes Dev. 2000; 14: 2501–
789 2514.
790 62. McMahon SB. MYC and the control of apoptosis. Cold Spring Harb Perspect Med.
791 2014; 4: a014407.
792 63. Yusa K, Zhou L, Li MA, Bradley A, Craig NL. A hyperactive piggyBac transposase for

mammalian applications. Proc Natl Acad Sci U S A. 2011; 108: 1531–1536.

64. Tabata S, Matsuda K, Nagai K, Izumi Y, Takahashi M, Motomura Y, et al. Nuclear NFκB activity balances purine metabolism in cellular senescence. bioRxiv. 2023. https://doi.org/10.1101/2023.04.18.536673.

65. Tabata S, Matsuda K, Soeda S, Nagai K, Izumi Y, Takahashi M, et al. NFκB dynamics-dependent epigenetic changes modulate inflammatory gene expression and induce cellular senescence. FEBS Journal. 2024; 291: 4951–4968.

66. Livak KJ, Schmittgen TD. Analysis of relative gene expression data using real-time quantitative PCR and the $2^{-\Delta\Delta CT}$ method. Methods. 2001; 25: 402–408.

67. Martin M. Cutadapt removes adapter sequences from high-throughput sequencing reads. EMBnet J. 2011; 17: 10–12.

68. Dobin A, Davis CA, Schlesinger F, Drenkow J, Zaleski C, Jha S, et al. STAR: Ultrafast universal RNA-seq aligner. Bioinformatics. 2013; 29: 15–21.

69. Liao Y, Smyth GK, Shi W. featureCounts: An efficient general purpose program for assigning sequence reads to genomic features. Bioinformatics. 2014; 30: 923–930.

70. Robinson MD, McCarthy DJ, Smyth GK. edgeR: A Bioconductor package for differential expression analysis of digital gene expression data. Bioinformatics. 2010; 26: 139–140.

71. R Core Team. A Language and Environment for Statistical Computing. (R Foundation for Statistical Computing, 2021). https://www.R-project.org/.

72. Korotkevich G, Sukhov V, Budin N, Shpak B, Artyomov MN, Sergushichev A. Fast gene set enrichment analysis. bioRxiv. 2021. https://doi.org/10.1101/060012.

73. Bolger AM, Lohse M, Usadel B. Trimmomatic: A flexible trimmer for Illumina sequence data. Bioinformatics. 2014; 30: 2114–2120.

74. Langmead B, Salzberg SL. Fast gapped-read alignment with Bowtie 2. Nat Methods.

818 2012; 9: 357–359.
819 75. Broad Institute. Picard, 2024. http://broadinstitute.github.io/picard.
820 76. Ramírez F, Ryan DP, Grüning B, Bhardwaj V, Kilpert F, Richter AS, et al. deepTools2: A
821 next generation web server for deep-sequencing data analysis. Nucleic Acids Res. 2016;
822 44: W160–W165.
823 77. Heinz S, Benner C, Spann N, Bertolino E, Lin YC, Laslo P, et al. Simple combinations
824 of lineage-determining transcription factors prime cis-regulatory elements required for
825 macrophage and B cell identities. Mol Cell. 2010; 38: 576–589.
826 78. Durinck S, Spellman PT, Birney E, Huber W. Mapping identifiers for the integration of
827 genomic datasets with the R/Bioconductor package biomaRt. Nat Protoc. 2009; 4: 1184–
828 1191.
829 79. Bailey TL, Johnson J, Grant CE, Noble WS. The MEME suite. Nucleic Acids Res. 2015;
830 43: W39–W49.
831 80. Castro-Mondragon JA, Riudavets-Puig R, Rauluseviciute I, Lemma RB, Turchi L,
832 Blanc-Mathieu R, et al. JASPAR 2022: The 9th release of the open-access database of
833 transcription factor binding profiles. Nucleic Acids Res. 2022; 50: D165–D173.
834

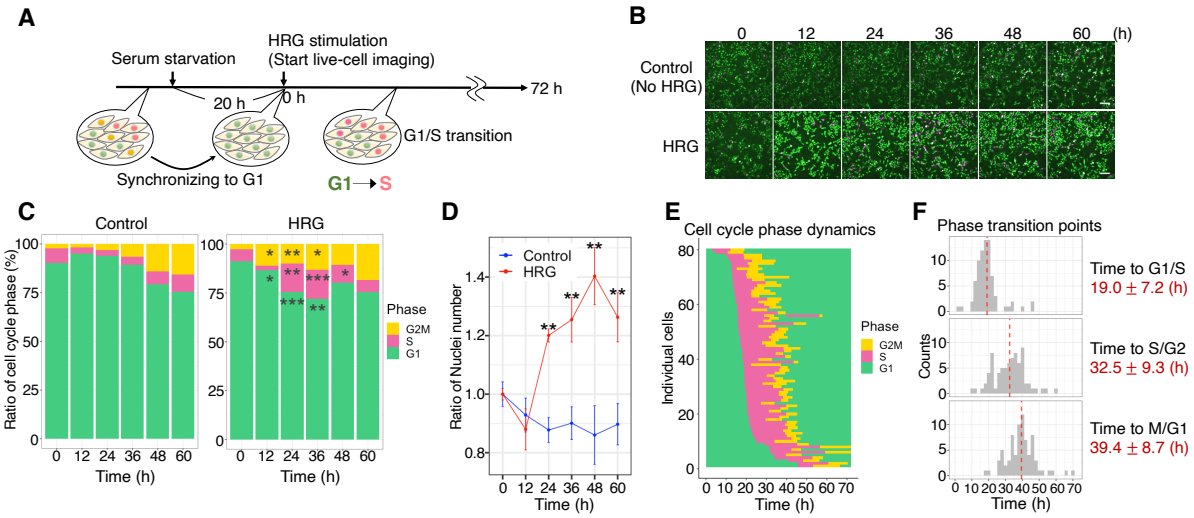

Fig. 1. G1/S transition occurs approximately 20 h after HRG stimulation. (A–F) MCF-7 cells stably expressing FUCCI. (**A**) Experimental scheme for live-cell imaging using FUCCI biosensor. (**B**) Images were captured every 20 min up to 72 h in conditions with or without 10 nM HRG. Scale bar: 100 µm. (**C**) Percentage distribution of each cell cycle phase (%) in each image; $n = 3$ fields per image. (**D**) The number of nuclei increased with each passing hour relative to the cell number at 0 h. (**E**) Cell cycle phase dynamics estimated based on Geminin and PIP fluorescence for individual cells followed up to 72 h; $n = 79$. (**F**) Histogram of cell cycle transition times for cells that completed the cell cycle within 72 h ($n = 77$), based on the results in (E). Red dotted lines indicate the mean ± SE of each transition time. In (C) and (D), $*P < 0.05$, $**P < 0.01$, $***P < 0.001$ (with respect to control and HRG; *t*-test).

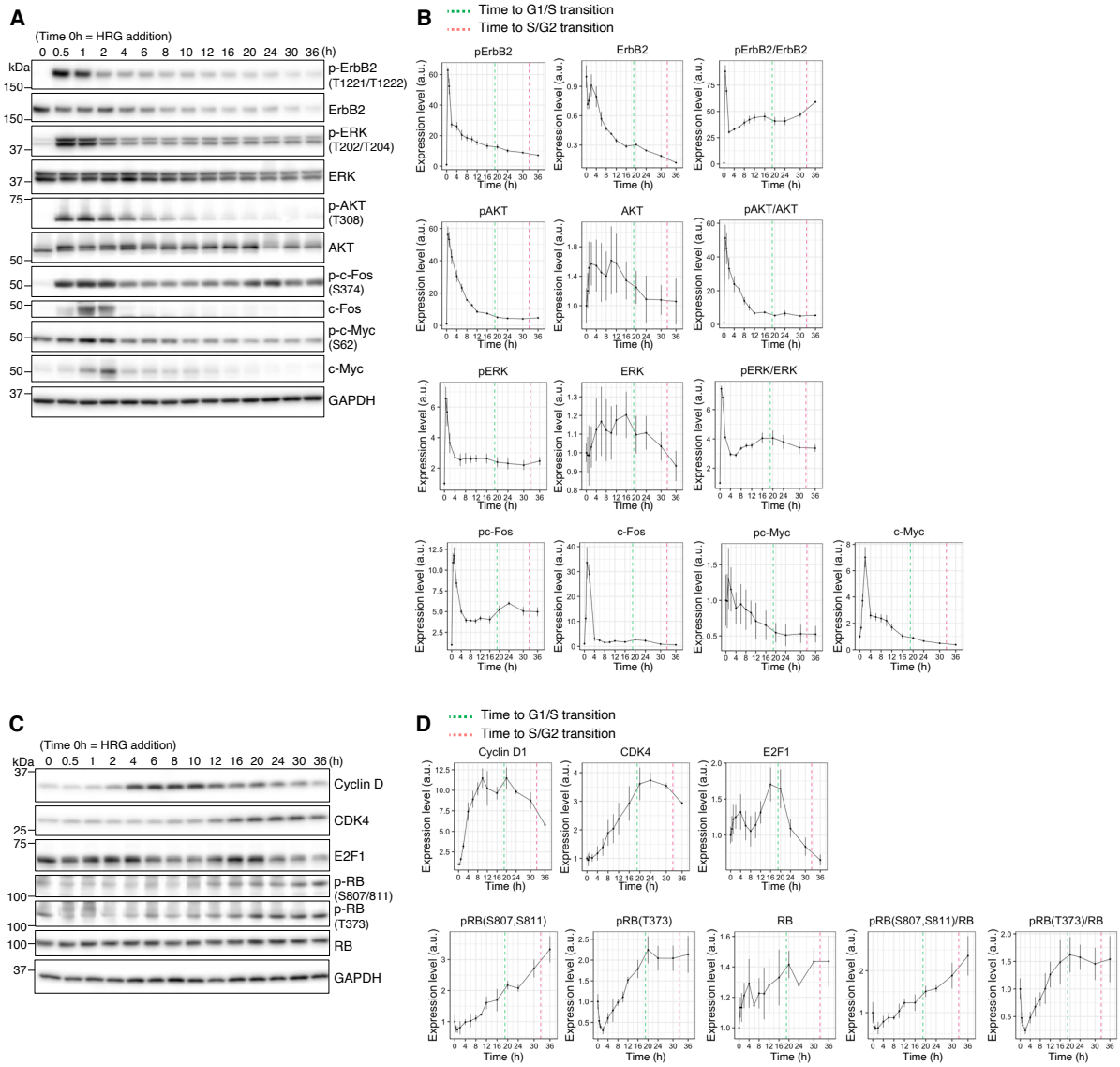

Fig. 2. Time-dependent expression of CDK4 and cyclin D1 in G1/S transition. (**A–D**) Dynamic changes in the expression or phosphorylation of individual proteins in MCF-7 cells stably expressing FUCCI, detected by western blotting up to 36 h after treatment with 10 nM HRG. (**A, B**) ErbB2 pathway proteins. (**C, D**) Proteins regulating G1/S transition. Protein and phosphorylation levels were normalized relative to those of GAPDH; $n = 3$.

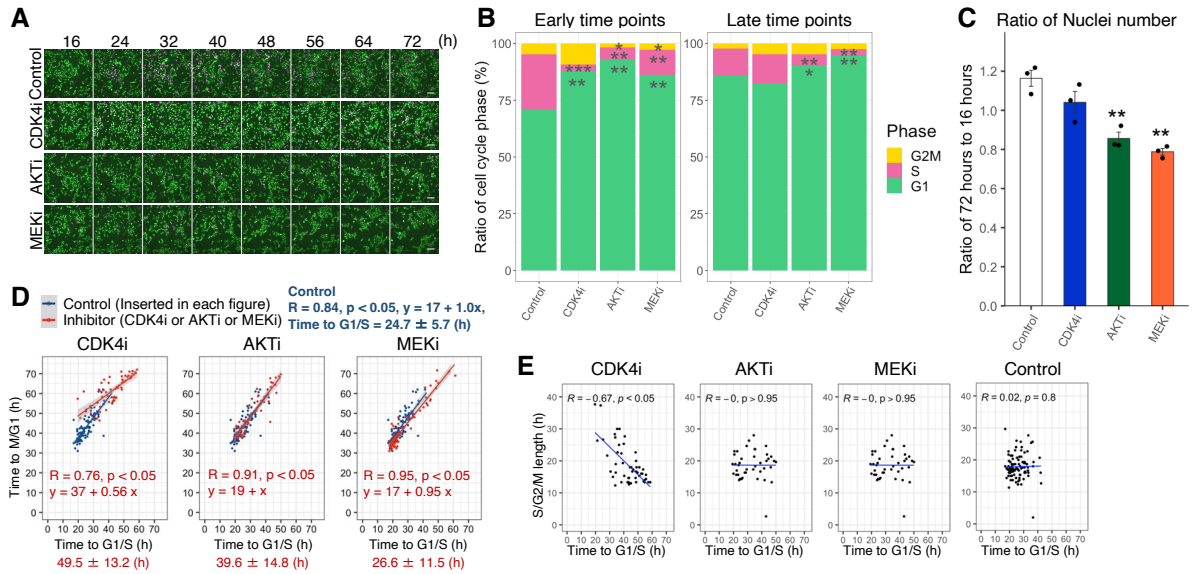

Fig. 3. A population subset enters the cell cycle even after CDK4 inhibition. (**A**) Each inhibitor (250 nM CDK4i; 600 nM AKTi; 500 nM MEKi) was used to treat the FUCCI stably expressing MCF-7 cells 12 h after HRG stimulation. Images were acquired every 20 min from 16 to 72 h after HRG stimulation. Scale bar: 100 µm. (**B**) Percentage distribution of each cell cycle phase (%) in the overall image at 32 h and 72 h after HRG stimulation; $n = 3$. (**C**) Increasing number of nuclei from 16 h to 72 h after HRG stimulation; $n = 3$. (**D**) Data from cells that completed the M/G1 transition within 72 h. Control, $n = 96$; CDK4i, $n = 52$; AKTi, $n = 42$; MEKi, $n = 75$. Times to G1/S (x-axis) and M/G1 (y-axis) transitions, with slope (s) and intercept (i) obtained from the regression equation. (**E**) Comparison of Pearson's coefficients using data from (D). In (B) to (C), $^*P < 0.05$, $^{**}P < 0.01$, $^{***}P < 0.001$ (with respect to control and each inhibitor; t-test).

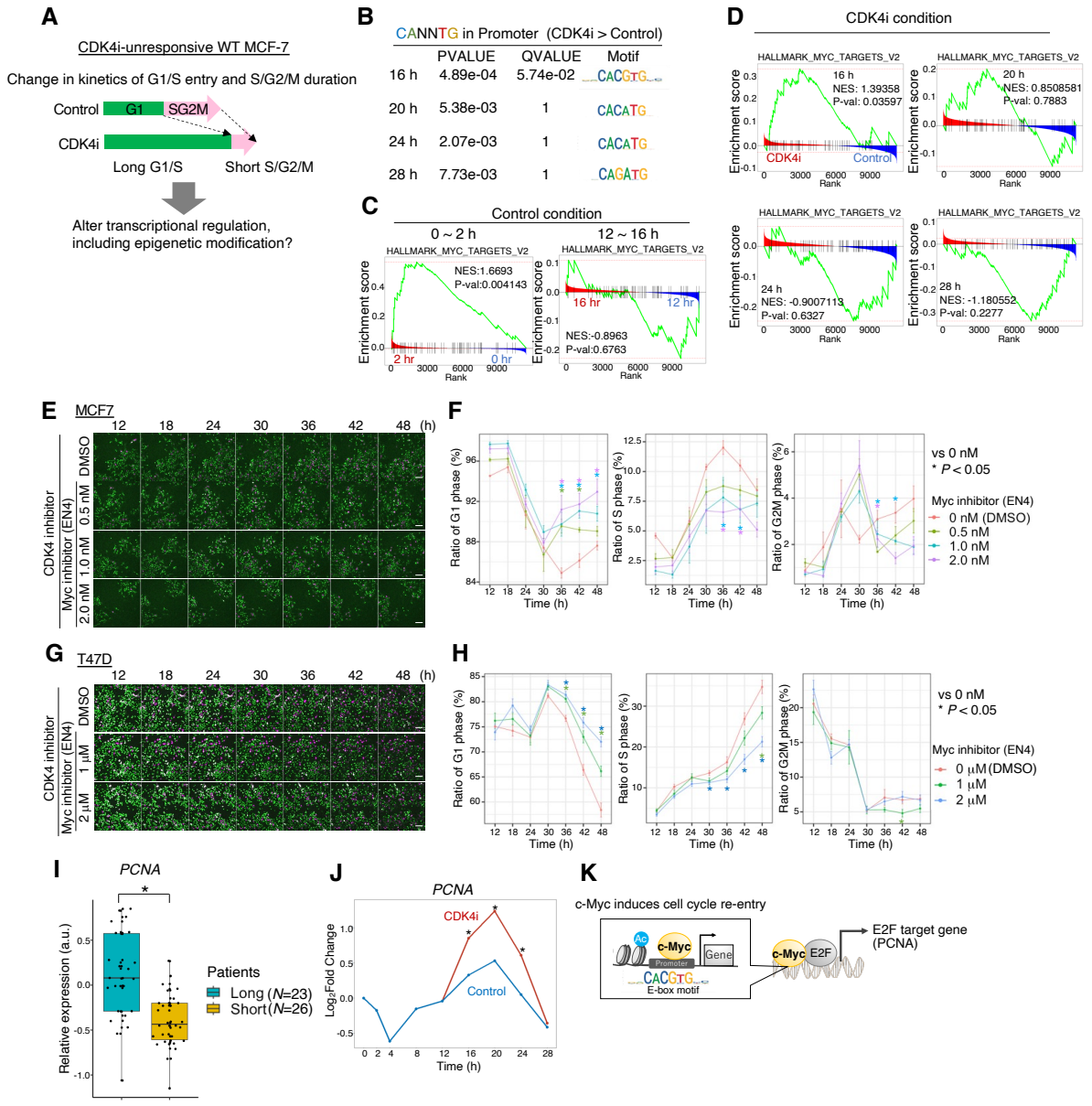

Fig. 4. CDK4i enhances c-Myc transcriptional activity via H3K27Ac modification. (**A**) Changes in cell-cycle distribution following CDK4 inhibition. (B–H, J) MCF-7 cells stably expressing FUCCI. (**B**) Motif-enrichment analysis of H3K27Ac modifications in the promoter region. E-box sequences (CANNTG) were enriched in the promoter region at all time points in the CDK4i group compared to the control group. (**C**) GSEA was performed using the Myc-target gene set (n = 58) obtained from the Human MSigDB Collections. Comparison between 0–2 h after HRG stimulation (NES = 1.6693, P = 0.004143) and near the R point (12–16 h; NES = –0.8963, P = 0.6763). (**D**) GSEA was performed using the Myc-target gene set (C). Comparison between CDK4i and control conditions every 4 h (16 h: NES = 1.39358, P = 0.03597; 20 h: NES = 0.8508581, P = 0.7883; 24 h: NES = –0.9007113, P = 0.6327; 28 h: NES = –1.180552, P = 0.2277). (**E–H**) After stimulation with 10 nM HRG for 11.5 h, cells were treated with 0 (DMSO)/0.5/1.0/2.0 nM EN4 (E, F) or 0 (DMSO)/1/2 mM

901 EN4 (G, H) for 30 min. Subsequently, MCF-7 (**E, F**) and T47D cells (**G, H**) were treated
902 with 250 nM CDK4i. Scale bar: 100 µm. The percentage distribution of each cell cycle phase
903 over time was quantified (**F, H**). (**I**) PCNA expression in microarray data from patients with
904 luminal A subtype breast cancer undergoing long-term (16 weeks, $n = 23$) or short-term (4
905 weeks, $n = 26$) treatment with CDK4/6i (adj. $P = 0.000132$). (**J**) *PCNA* mRNA expression in
906 RNA-seq data. (**K**) Increased c-Myc activity induces cell cycle re-entry to promote E2F
907 target gene expression. In (F) and (H), $*P < 0.05$ (with respect to control and each inhibitor;
908 *t*-test). In (I), $*P < 0.05$ (calculated using the Benjamini–Hochberg method). In (J), $*P < 0.05$
909 (calculated using EdgeR).

910

911

912

913

914

915

916

917

918

919

920

921

922

923

924

925

926

927

928

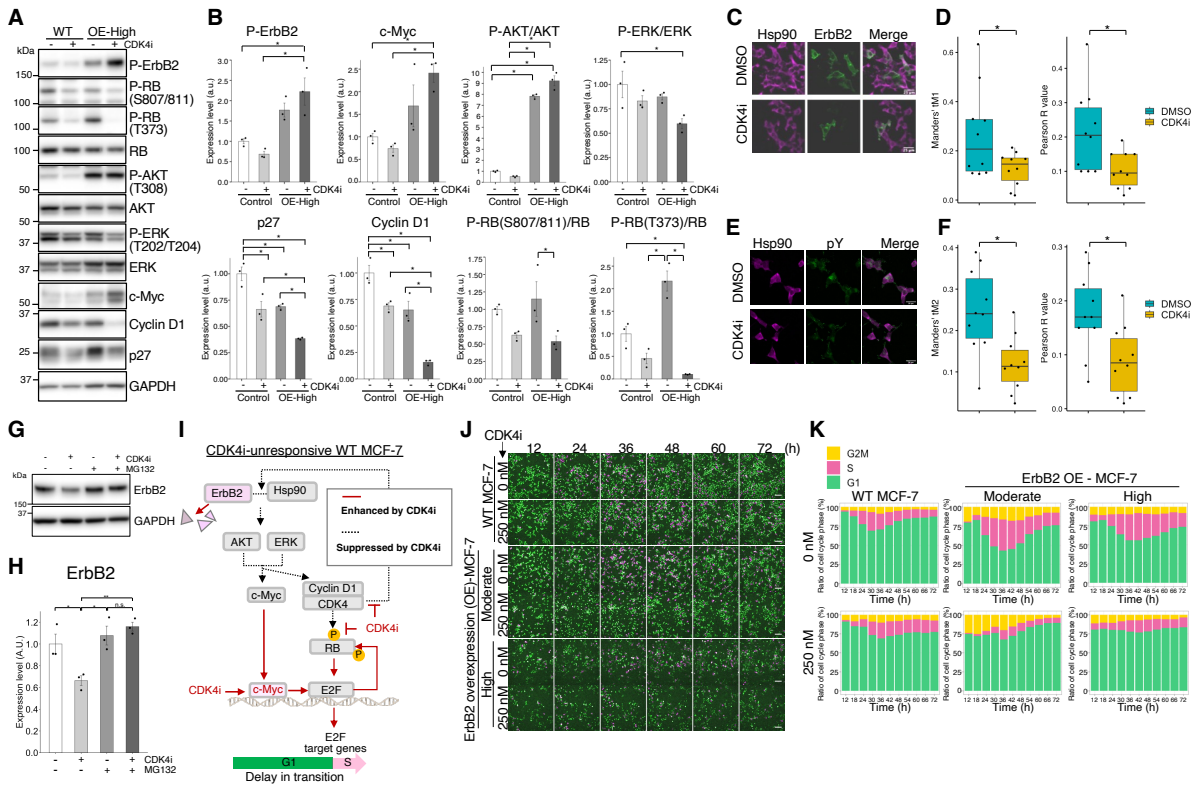

929

930 **Fig. 5. High ErbB2 expression induces cell cycle arrest by repressing cyclin D1**
931 **expression via c-Myc under CDK4 inhibition.** (**A, B**) WT MCF-7 and ErbB2-
932 overexpressing MCF-7 cells (high levels) were treated with CDK4i or DMSO 12 h after
933 HRG stimulation and harvested 24 h after HRG stimulation. Western blotting of (A) p-
934 ErbB2, p-RB (Ser$^{807/811}$), p-RB (Thr^{373}), RB, p-AKT (Thr^{308}), AKT, p-ERK (Thr^{202}/Thr^{204}),
935 ERK, c-Myc, cyclin D1, and p27 expression (in control cells, i.e., DMSO treatment) after
936 normalization with GAPDH expression (B). (**C–F**) ErbB2-overexpressing cells (moderate)
937 were individually treated with 250 nM CDK4i or DMSO (no treatment) 12 h after stimulation
938 with 10 nM HRG and fixed 16 h after stimulation with 10 nM HRG (CDK4i or DMSO
939 addition 4 h later). Hsp90 and ErbB2 were co-immunostained. Scale bar: 25 µm (C). Co-
940 localization rate of Hsp90 and ErbB2 based on Mander's tM1 and Pearson's R values
941 determined using Coloc 2 plugin of Image J; n = 10 (D). Hsp90 and PY100 were co-
942 immunostained. Scale bar: 25 µm (E). Co-localization rate of Hsp90 and PY100 based on
943 Mander's tM2 and Pearson's R values; n = 10 (F). (**G, H**) FUCCI stably expressing MCF-7
944 cells were treated with CDK4i or DMSO (control) as well as 10 mM MG132 12 h after
945 stimulation with 10 nM HRG and collected 8 h later. (**G**) Expression of ErbB2 and GAPDH
946 determined by western blotting. (**H**) ErbB2 expression normalized to GAPDH expression; n
947 = 3. (**I**) In CDK4i-unresponsive WT MCF-7 cells, the loss of ErbB2 protein stability impairs
948 the regulation of c-Myc-mediated G1/S transition, leading to the delayed G1/S transition. (**J**)
949 WT MCF-7 and ErbB2-overexpressing cells (moderate and high levels) were individually
950 treated with 250 nM CDK4i or DMSO (no treatment) 12 h after stimulation with 10 nM

951 HRG, and images were acquired every 20 min until 72 h after stimulation. Scale bar: 100 μm.
952 (**K**) Images in (J) were analyzed to determine the proportion (%) of each cell cycle phase in
953 the entire set of images; $n = 3$. In (B) and (H), $*P < 0.05$ (Tukey's test). In (D) and (F), $*P <$
954 0.05 (with respect to control and CDK4i; *t*-test).
955
956
957
958
959
960
961
962
963
964
965
966
967
968
969
970
971
972
973
974
975
976
977

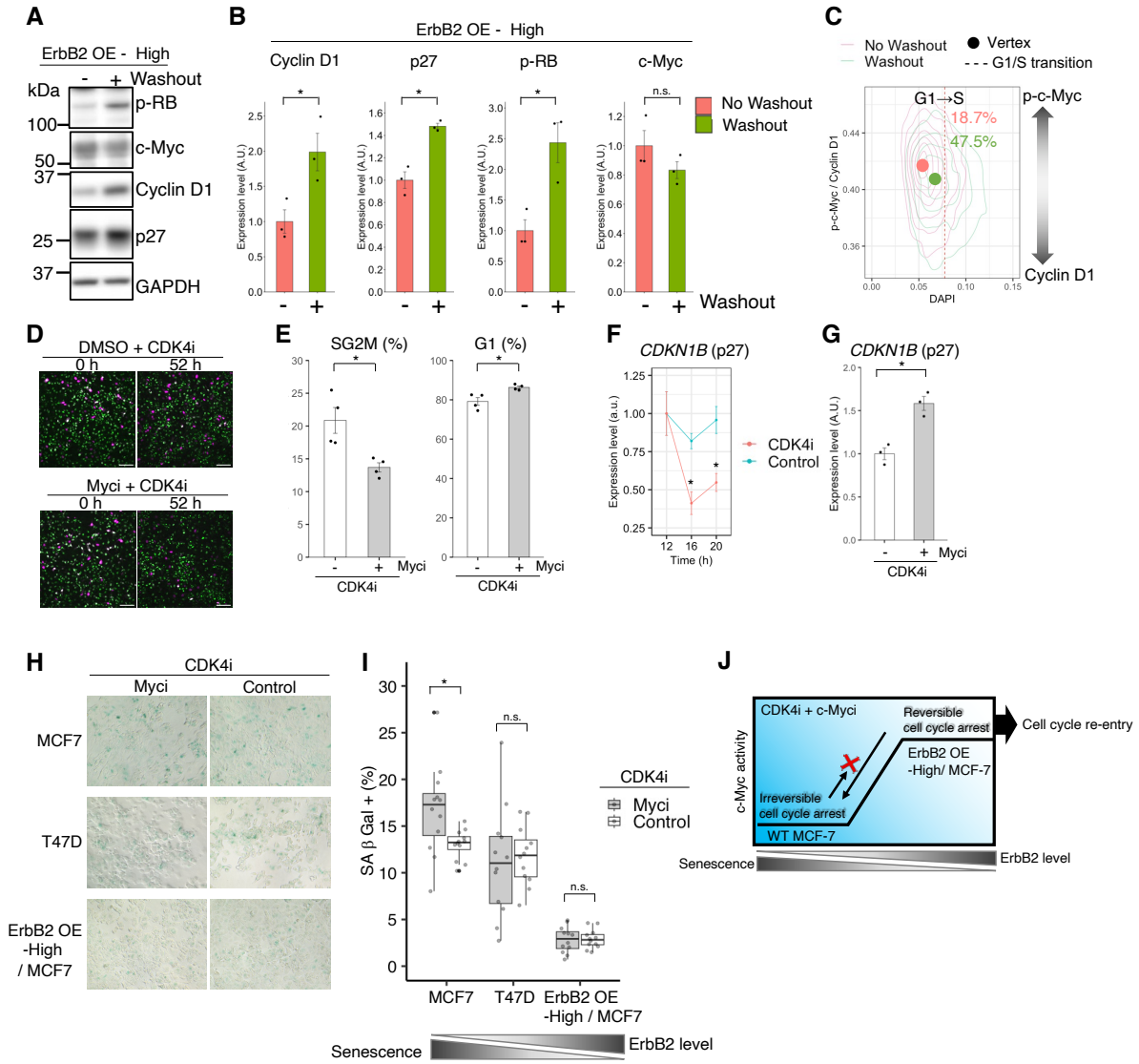

Fig. 6. Reversible cell cycle arrest is maintained under c-Myc transcriptional activity. (**A–G**) MCF-7 cells overexpressing ErbB2 (high levels). (**A, B**) Cells were treated with 250 nM CDK4i 12 h after HRG stimulation, subjected to a wash/no-wash treatment 4 h later, and harvested 40 h after HRG stimulation. Western blotting results showing the expression of p-RB, c-Myc, cyclin D1, p27, and GAPDH. After individually normalizing the proteins relative to GAPDH, the ratio to the no-wash condition was quantified; $n = 3$. (**C**) Washing operations were performed under the same conditions as in (A, B); cells were fixed 40 h after HRG stimulation and immunostained with p-c-Myc and cyclin D1 antibodies together with DAPI; $n = 3\,859$. A higher value on the y-axis indicates that the amount of p-c-Myc in one cell was greater than that of cyclin D1. The circle shows the vertex of each histogram, and the red dotted line indicates the G1/S transition time point. (**D, E**) Cells were pre-treated for 30 min with/without 64 nM c-Myc inhibitor (EN4) 11.5 h after HRG stimulation. The cells were then incubated with 250 nM CDK4i for 8 h, washed, and imaged 52 h later (72 h after HRG

stimulation, D). (**E**) Percentage distributions of G1 and S/G2/M phases based on the images in (D); $n = 3$. Scale bar: 100 µm. (**F**) Cells were treated with 250 nM CDK4i or DMSO (control) 12 h after HRG stimulation and p27 mRNA levels up to 20 h after HRG stimulation were examined by qPCR; $n = 3$. (**G**) After the cells were treated with or without EN4 under the same conditions as in (D–E), RNA was collected 8 h after treatment with inhibitors, and *CDKN1B* mRNA levels were examined by qPCR; $n = 3$. (**H**) WT MCF-7, WT T47D, and ErbB2 (high) OE MCF-7 cells were pre-treated for 30 min with/without 4 mM c-Myc inhibitor (EN4) 11.5 h after HRG stimulation, incubated with 250 nM CDK4i for 6 d, and SA-β-Gal staining was assessed. (**I**) Percentage SA-β-Gal-stained cells based on the images in (H); $n = 12$. (**J**) ErbB2 levels modulate the irreversibility of the G1/S transition under CDK4i treatment. In (B), (E), (F), (G), (I) $^*P < 0.05$ (with respect to control and each inhibitor; *t*-test).

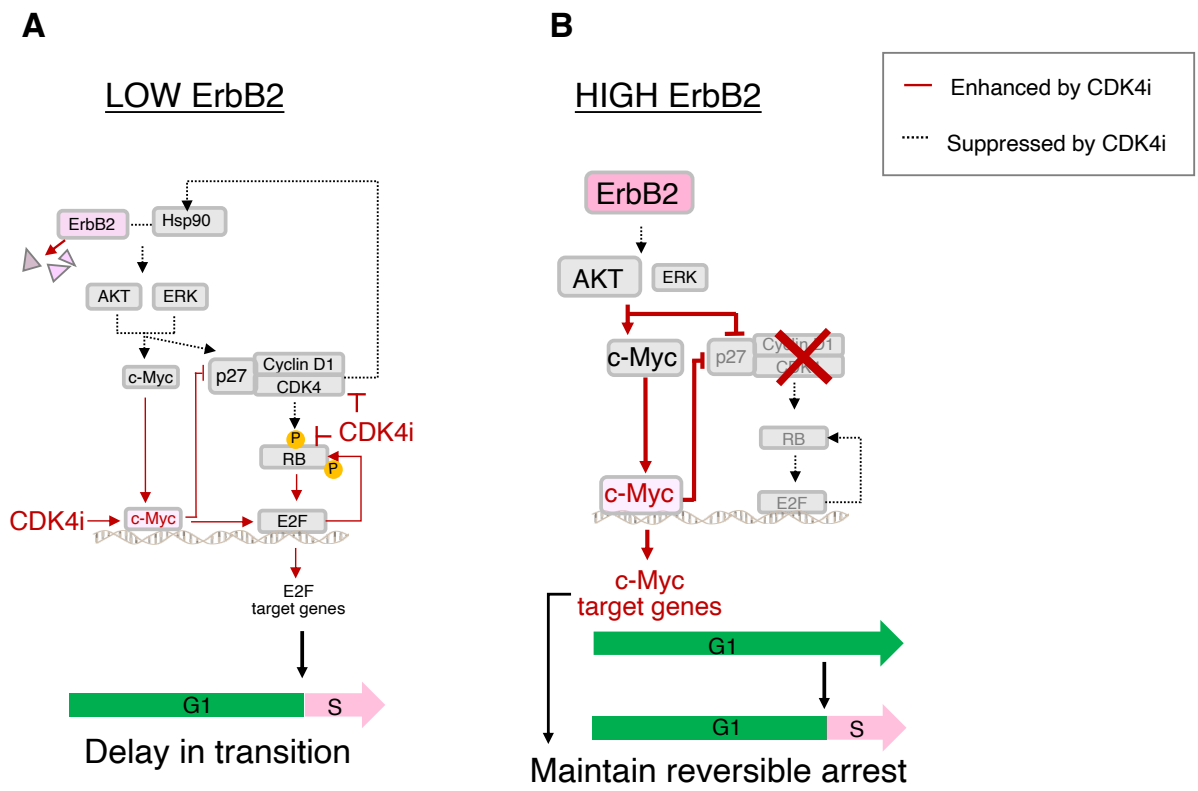

Fig. 7. Proposed model the ErbB2 receptor regulation during G1/S transition via cyclin D1 and c-Myc in CDK4i non-responsive cells. (**A**) In low ErbB2-expressing cells, CDK4 inhibition leads to reduced pathway activity due to ErbB2 degradation via Hsp90 dis-colocalization. This attenuates the transcriptional activity of c-Myc activated by epigenetic changes. Consequently, a subpopulation of cells unresponsive to CDK4i exhibits a delayed G1/S transition. (**B**) In high ErbB2-expressing cells, increased AKT activity leads to increased c-Myc expression. Subsequently, the expression of p27, which is critical for the stability of cyclin D1/CDK4 during the G1 phase, is suppressed by c-Myc, resulting in cell cycle arrest after CDK4 inhibition. This arrest is reversibly maintained by the strong transcriptional activity of c-Myc, ultimately sustaining survival signals.